PARAMETRIC STUDIES OF TIG WELDING PROCESS PARAMETERS ON 409M FERRITIC STAINLESS STEEL BY USING GREY-TAGUCHI METHOD.

By

Sayantan Sinha Biswas

Examination Roll No. – M4MEC23016

Registration No. - 160289

Class Roll No.- 002111202026

Under the guidance of

Dr. NABENDU GHOSH
Department of Mechanical Engineering
Jadavpur University

&

Prof. (Dr.) BUDDHADEB ORAON
Department of Mechanical Engineering
Jadavpur University

THESIS

SUBMITED IN PARTIAL FULFILMENT OF THE REQUIREMENTS FOR THE

DEGREE OF

MASTER OF MECHANICAL ENGINEERING

IN THE FACULTY OF ENGINEERING AND TECHNOLOGY

JADAVPUR UNIVERSITY

DEPARTMENT OF MECHANICAL ENGINEERING
JADAVPUR UNIVERSITY
KOLKATA – 700032
2023

DECLARATION OF ORIGINALITY AND COMPLIANCE OF ACADEMIC ETHICS

I, Mr. Sayantan Sinha Biswas do hereby declare that this thesis entitled PARAMETRIC STUDIES OF TIG WELDING PROCESS PARAMETERS ON 409M FERRITIC STANLESS STEEL BY USING GREY-TAGICHI METHOD contains literature survey and original research work done by the undersigned candidate as part of Master of Mechanical Engineering studies.

All information in this thesis have been obtained and presented in accordance with existing academic rules and ethical conduct. I declare that, as required by these rules and conduct, I have fully cited and referred all materials and results that are not original to this work.

Signature of Candidate:

Date:

JADAVPUR UNIVERSITY

Raja S.C. Mallick Road, Kolkata 700032, West Bengal, India

FACULTY OF ENGINEERING AND TECHNOLOGY

CERTIFICATE OF RECOMMENDATION

We hereby recommend that the thesis prepared under our supervision by **Mr. Sayantan Sinha Biswas** examination roll number M4MEC23016, entitled "**PARAMETRIC STUDIES OF TIG WELDING PROCESS PARAMETERS ON 409M FERRITIC STAINLESS STEEL BY USING GREY-TAGUCHI METHOD**" be accepted in partial fulfilment of the requirements for the degree of Master of Mechanical Engineering.

To the best of our knowledge, the matter embodied in the thesis has not been submitted to any other University/Institute for the award of any degree or diploma.

_____

THESIS SUPERVISOR

Dr. Nabendu Ghosh

Assistant Professor
Department of Mechanical Engineering,
Jadavpur University, Kolkata 700032, India

_ _____

THESIS CO-SUPERVISOR

Prof. (Dr.) Buddhadeb Oraon

Professor,
Department of Mechanical Engineering,
Jadavpur University, Kolkata 700032, India

_____

Prof. (Dr.) Ardhendu Ghosal
Dean,
Faculty Council of Engineering & Technology,
Jadavpur University, Kolkata 700032, India

_____

Prof. (Dr.) Amit Karmakar
Head of the department,
Department of MechanicalEngineering,
Jadavpur University, Kolkata 700032, India

JADAVPUR UNIVERSITY

Raja S.C. Mallick Road, Kolkata 700032, West Bengal, India

FACULTY OF ENGINEERING AND TECHNOLOGY

CERTIFICATE OF APPROVAL

The foregoing thesis is hereby approved as a credible study of an engineering subject carried out and presented in a manner satisfactory to warrant its acceptance as a pre-requisite to the degree for which it has been submitted. It is understood that by this approval the undersigned do not endorse or approve any statement made, opinion expressed or conclusion drawn therein but approve the thesis only for the purpose for which it is submitted.

_____

Committee

On Final examination

_____

For evaluation of the thesis

_____

Signature (s) of the examiners

ACKNOWLEDGEMENT

The author gratefully expresses his sincere gratitude to the thesis supervisors **Dr. Nabendu Ghosh**, Assistant Professor and **Prof. (Dr.) Buddhadeb Oraon**, Professor Mechanical Engineering Department, Jadavpur University, Kolkata for their invaluable guidance, suggestions and encouragement in the course ofthe present work.

The author is indebted to **Variable Energy Cyclotron Centre (VECC) is a premier R & D unit of the Department of Atomic Energy**, faculty members of Mechanical Engineering Department, Jadavpur University, for their invaluable help and advice to this thesis work from time to time. The author acknowledges the help rendered by **Prof. (Dr.) Titas Nandi** Superintendent, Blue Earth Machine Shop, Mechanical Engineering Department, Jadavpur University. The author is very much grateful to **Prof. Sumanta Neogi**, Professor and Ex- Head, Mechanical Engineering Department, Jadavpur University and **Prof. (Dr.) Amit Karmakar,** Professor and Head, Mechanical Engineering Department, Jadavpur University for giving encouragement for completing the thesis.

The author is indebted to his friend at Mechanical Engineering Department of Jadavpur University. The author would like to convey thanks to **Mr. Angshuman Roy**, PhD Research Scholar of Power Engineering Department, for his constant support and help.

The author will fail in his duty if he does not offer thanks to all his friends, seniors and class- mates for presenting the thesis in the present form.

The author pays his sensible appreciation to all those who submitted the invaluable database of information in the internet and also to those who are maintaining such invaluable database records, providing a great help for the researchers in the field of science and technology.

Mr. Sayantan Sinha Biswas

CONTENTS

CHAPTER 1

1.1 INTRODUCTION

When two pieces of metal are joined together during welding, filler metal may or may not be used, along with heat and/or force. Shielding gases, pastes, or powders for welding, for instance, can aid to facilitate it. It comes from outside to provide the energy needed for welding.Welding has a long and illustrious history. The Sumerians began welding metals together in 4000 BC. They welded gold pieces together. The next significant development in welding technology was not made for a very long period after that. The Egyptians built copper lines by fire welding approximately 2700 BC. Jewellery creation also involved fire welding. Welding technology was revolutionized by discoveries such as Guerick, Leibniz, and Kleist in 1745.But only between 1880 and 1887 did the breakthrough occur. The arc welding process was developed during this time by the Russian inventor Benardos Nikolai Nikolaevich. For the first time ever, he used an electric arc to unite two metal components. Between a workpiece and a carbon electrode, he created an arc to demonstrate his theory for the first time in 1881 in Paris. In 1908, Oskar Kjellberg created coated electrodes to improve the welded joints' quality. The majority of totally and partially mechanical techniques currently in use are all substantially more recent:

- Tungsten Inert Gas (TIG) Welding, 1936
- Submerged Arc Welding, 1936
- Metal inert gas (MIG) welding, 1948
- Plasma welding ,1960
- Laser welding, 1970

A method of joining that is extremely systematic is welding. Figure 1.1 recognises four distinct types of joining processes, including joining by forming, brazing, welding, and adhesive bonding

.

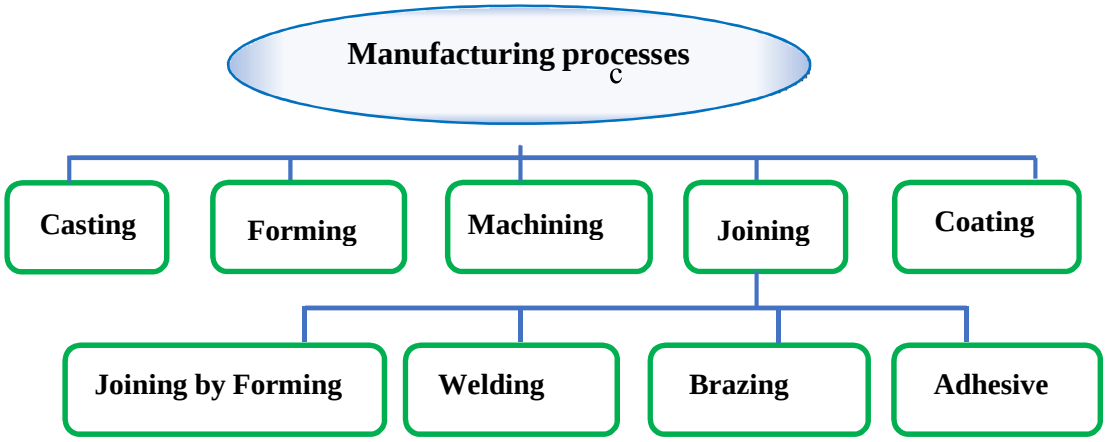

Fig. 1.1 Categorization of joining techniques in manufacturing processes

1.2 DIFFERENT TYPE OF WELDING PROCESSES

Welding procedures can be categorised into the following groups, according to the heat source used:

An arc is created when two electrodes come into contact. An ionised hot gas called plasma conducts electricity. Welding arcs, also referred to as electric arcs, are frequently created between a thin rod (or wire) and a plate. A welding arc typically runs at a high current, low voltage discharge of 10 to 50 volts. In welding circuits, arcs act as load resistors.

Gas Welding: The work components are melted together and merged during the gas welding process employing a concentrated, high-temperature flame created by gas combustion or a gas combination. For proper welding, a filler substance is utilised externally. The most popular method of gas welding is oxygen-acetylene welding, which involves the reaction of acetylene and oxygen to produce heat.

Resistance Welding: In resistance welding, heat is generated when a significant current (between 1000 and 100,000 A) travels through the resistance that is created when two metal surfaces come into contact. Spot welding, the most common variety of resistance welding, employs a pointed electrode. Continuous type spot resistance welding can be used for seam welding when a wheel-shaped electrode is used.

High Energy Beam Welding: In this kind of welding, the work components are melted and joined together using a focused energy beam of high intensity, like a laser or electron beam. These kinds of welding are typically employed for precision welding, welding of sophisticated materials, or occasionally welding of materials that are not compatible with each other using standard welding processes.

Solid-State Welding: The materials to be bonded in the work piece do not need to be melted during solid-state welding techniques. Electromagnetic pulse welding, friction welding, ultrasonic welding, friction-stir welding, etc are examples of common solid-state welding techniques.

Arc Welding: Among all of these welding procedures, arc welding is one that is frequently utilised for a variety of materials. Typical arc welding process types include:

Shielded Metal Arc Welding (SMAW) or Manual Metal Arc Welding: The consumable electrode that is utilized in this sort of arc welding technique is coated in flux. As the electrode melts, the flux degrades, producing slag that covers the flowing filler metal as it travels from the electrode to the weld pool, shielding gas that protects the weld area from gases like oxygen and other gases, and shielding gas that melts the electrode. Slag floats to the top of the weld pool when the weld cures to protect it from the atmosphere.

Gas Metal Arc Welding (GMAW) or Metal inert or active gas welding (MIG/MAG):

A continuous, reusable wire electrode is used during this type of welding technique. A shielding gas, usually argon or sporadically a mixture of argon and carbon dioxide, is given to the weld zone by a welding gun.

Gas Tungsten Arc Welding (GTAW) or Tungsten Inert Gas (TIG): GTAW or TIG

The weld is produced using a non-consumable tungsten electrode during the welding process. A shielding gas, usually argon or helium or occasionally a combination of argon and helium, is used to protect the weld region from the atmosphere. A filler metal can also be manually fed for appropriate welding in GTAW welding process, sometimes known as TIG welding, was created during World War II. The technology of TIG welding has made it possible to weld materials that were previously impossible, such aluminium and magnesium. Today, TIG is used on a wide range of metals, including titanium alloy, stainless steel, mild steel, and high tensile steels. TIG welding power supplies have advanced alongside

other welding systems, going from simple transformer types to the highly electronic controlled power sources we see today.

1.3 BASIC MECHANISM OF TIG WELDING:

The TIG welding process produces a weld using an inert tungsten electrode. Typically, a filler metal is used, and an inert shielding gas (helium or argon) protects the weld area from the atmosphere. After being delivered from the power source (rectifier), the power is then given to a tungsten electrode that is placed into the hand piece through a hand-piece or welding torch. Using a constant-current welding power source, an electric arc is then produced between the tungsten electrode and the work piece, transferring energy across the arc through a column of highly ionised gas and metal vapours. An inert gas shields the tungsten electrode and welding region from the surrounding air. Temperatures of up to 20,000 °C can be produced by an electric arc, and this focused heat can be used to combine and melt two different types of materials. The base metal can be joined using either a weld pool or filler material. Figure 1.2 below displays a schematic illustration of TIG welding and its mechanism.

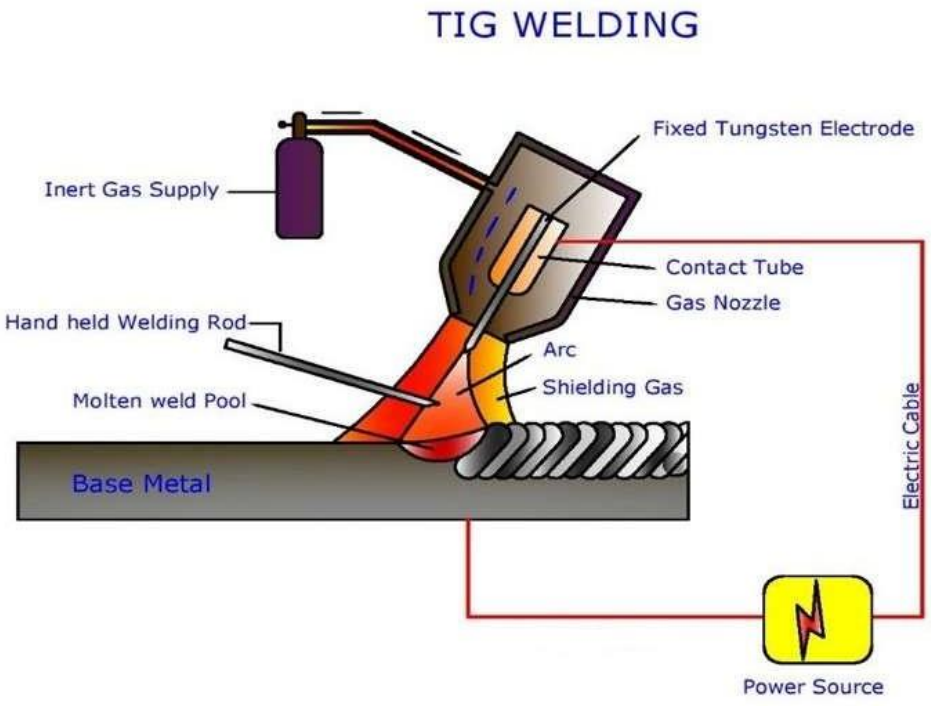

Fig. 1.2 TIG Welding System Schematic Diagram.

Common tungsten electrode sizes range from 0.5 mm to 6.4 mm in diameter and 150-200 mm in length. The ability of an electrode to transmit current depends on whether it is connected to the positive or negative terminal of a DC power source. The power supply required to maintain the TIG arc has a drooping or steady current characteristic that generates an output that is essentially constant while the arc length fluctuates across a number of millimeters. As a result, the welding current is unaffected by the normal arc length variations that occur during manual welding. The capacity to restrict the current to the predetermined value when the electrode is shorted to the work piece is equally crucial; otherwise, an extremely high current will flow, damaging the electrode. The open circuit voltage of the power source varies from 60 to 80 V.

1.4 TYPES OF WELDING CURRENT USED IN TIG WELDING

a) DCSP (Direct Current Straight Polarity): Direct current is used while TIG welding in this manner. The negative power supply connection is connected to the tungsten electrode. The most typical and extensively used method of DC welding is this kind of connection. Only 30% of the welding energy (heat) will reach the tungsten since it is connected to the negative terminal. The resulting weld has a small profile and good penetration.

b) DCRP (Direct Current Reverse Polarity): The positive terminal of the power supply is connected to the tungsten electrode in this sort of TIG welding configuration. Because the tungsten receives the majority of the heat and can rapidly overheat and burn away, this sort of connection is utilised relatively infrequently. When used on very light material at low Amp, DCRP creates a shallow, wide profile.

c) AC (Alternating Current): For the vast majority of white metals, such as aluminium and magnesium, it is the recommended welding current. As the AC wave moves from one side to the other, the heat input to the tungsten is averaged out. Electrons will flow from the base material to the tungsten during the half cycle, which is when the tungsten electrode is positive. Any oxide skin on the base material will lift as a result. The cleaning half of the waveform refers to this side. Electrons will migrate from the welding tungsten electrode to the base material as the wave advances to the point where the tungsten electrode turns negative. The penetration half of the AC wave forms refers to this side of the cycle.

d) Alternating Current with Square Wave: Modern electricity has made it possible to construct AC welding machines using the square wave waveform. The square wave is easier to manage, and each side of the wave can provide greater cleaning and penetration during the welding cycle.

1.5 ADVANTAGES OF TIG WELDING

The following are some particular benefits of TIG welding over other arc welding processes:

i) A concentrated narrow arc

ii) Capable of joining ferrous and non-ferrous metals together.

ii) Uses shielding gas to protect the tungsten electrode and weld pool, leaving no flux or slag behind.

iv) When TIG welding, there are no fumes or sputter.

1.6 APPLICATIONS OF TIG WELDING

The ideal metal plates for TIG welding are those with a thickness of 5 to 6 mm. thicker plates can be joined using TIG multi-pass welding, although doing so results in substantial heat inputs that change the mechanical properties of the base metal. TIG welding allows for a high degree of heat input and filler addition control, which results in the production of welds of exceptional quality. TIG welding may be done in any position and is effective for joining tubes and pipes. TIG welding is a clean, highly controlled procedure that occasionally requires no finishing at all. It is possible to employ this welding technique in both manual and mechanised operations. TIG welding is frequently used in so-called high-tech applications, such as those related to

- The Nuclear Sector
- Aircraft Sector
- Food Processing Sector
- Maintenance and Repair Operations
- Precision Manufacturing Industry
- Automotive Industries.

1.7 PROCESS PARAMETERS USED IN TIG WELDING

The following list includes the variables that have an impact on the TIG welding process's quality and results.

a) Welding Current: In TIG welding, a higher current can cause spatter and work piece damage. Once more, using a lower current level for TIG welding causes the filler wire to stick. Since high temperatures must be applied for longer periods of time to deposit the same amount of filler materials, bigger heat impacted areas can occasionally be discovered for lower welding current. The voltage will fluctuate in fixed current mode in order to keep the arc current constant.

b) Welding Voltage: Welding Depending on the TIG welding equipment, the voltage can either be fixed or adjustable. A large working tip distance range and simple arc initiation are both made possible by a high starting voltage. High voltage can cause significant variations in the quality of the weld.

c) Inert Gases: The optimum shielding gas to utilise depends on the working metals, and this decision affects welding costs, weld temperatures, arc stability, weld speeds, splatter, electrode life, etc. It also affects the final weld penetration depth and surface profile, as well as the porosity, corrosion resistance, strength, hardness, and brittleness of the weld material. Both helium and argon are capable of being used for TIG welding processes. For welding exceedingly thin materials, pure argon is employed. An arc made by argon often runs more silently and smoothly. Argon's use results in arc penetration that is less intense than Helium's. Because of these factors, argon is preferred in most applications, with the exception of those where more heat and penetration are required to weld thicker areas of metals with high heat conductivity.

d) Welding speed: An essential factor in TIG welding is welding speed. Increased welding speed leads in less weld reinforcement and decreased penetration of the weld because the amount of power or heat input per unit length of the weld reduces. The bead size and penetration of the weld are primarily controlled by the welding speed or travel speed. It and current are interconnected. Lesser welding speed reduces the tendency of porosity while excessively high welding speed increases the tendency of undercut, porosity, and irregular bead structures.

1.8 INSPECTION AND TESTING OF WELDS

Good quality weld is preferred to satisfy demand, and inspection at every stage is necessary to look for flaws or incorrect procedures. To ensure proper welding, there are three processes to go through. Keeping input parameters (such as gas flow rate, welding current, arc gap, welding speed, and welding voltage) that effect of heat input in the welding process, defending the weld pool from contaminating air, and removing slag, peening, and post-welding treatment are all important before welding. A quality weld can be achieved by remembering these three procedures. The prepared weld is subjected to several

examinations in the form of various tests to determine how well it has been prepared. Destructive and non-destructive welding joint testing techniques are available.

1.9 NON-DESTRUCTIVE TEST

Non-destructive testing for welds that are visual, ultrasonic, and radiographic (X-ray). Weld-meant defects can be found using any non-destructive test. In many cases, visual inspection is the quickest and most affordable technique. Although discontinuities are sometimes obvious, a pretty weld does not always imply a good weld. Surface crack detection is used to find microscopic cracks, seams, porosity, and other surface-breaking discontinuities. One of the most popular techniques for spotting surface fractures is liquid penetrant testing. Only discontinuities that are surface-breaking, or exposed to the penetrant's surface, can be found using this form of testing. Internal porosity or fusion flaws that are completely sealed inside the weld body cannot be found by it. Because incorrect results might make interpretation difficult, it is not appropriate for testing rough or porous materials. This kind of inspection is more likely to find hairline cracks and small surface porosities than an unaided eye check. Both ferrous and nonferrous materials can be inspected using this procedure. During a fluorescent penetrant inspection, the inspection area is covered with a highly fluorescent liquid. The penetrant is brought to the surface by the developer, and the weld is examined under a black light. The luminous substance can be contrasted with the object to help inspectors find penetrant traces on surfaces.

Radiographic physical weld testing reveals flaws such blowholes, cracks, and incorrect fusion zones. In order to record the radiant energy transmitted and allow X-rays and gamma rays to flow through metal and other opaque materials, radiography depends on this property. On one side, we store a sensitive emulsion x-ray film, and on the other, an x-ray tube.

1.10 DESTRUCTIVE TEST

In order to analyse a weld's qualities, destructive weld testing includes physically destroying the weld. This testing approach is frequently employed in numerous applications. These consist of qualification of the welding process, qualification of the welder's performance, inspection of production weld samples, inspection of research samples, and failure analysis. Weld integrity is evaluated via destructive weld testing. They require cutting the welded component into sections and breaking it apart to evaluate its mechanical and physical characteristics. We'll discuss guided bend testing, transverse stress tests, fillet weld break tests, and macro etch tests. We'll examine their applications and the weld features they're designed to spot.

Tensile Strength Test: This test measures the tensile strength of a welded junction. It is necessary to test a piece of the welded plate in the testing device's jaws. The test sample's breadth and thickness are measured beforehand. Before testing and computing, multiply the width and thickness. The specimen for the physical tensile weld strength test is now set up on a machine that will pull so hard that it will break. There are both stationary and portable testing tools available. A portable hydraulic testing device that can pull and bend the specimen is shown in the illustration. While this machine is being tested, the load in pounds is visible on the gauge. The balancing beam load is shown on the stationary machine. At the break, the load is always recorded. Tensile strength is calculated by dividing the specimen's break load by its initial cross-sectional area. At least 90% of the base metal's tensile strength must be pulled by the specimen. Shearing strength of longitudinal and transverse fillet welds is determined by the tensile stress of test samples. The maximum load is noted as the test sample ruptures. Using this test, you can find out the yield strength, ultimate tensile strength, ductility, % elongation, Young's modulus, and other properties of the weld joint. The specimen is bent to a predetermined bend radius in the bend test method. The ductility and strength of welded joints are evaluated using bend tests. Typically, they are carried out using plunger testing equipment or wrap-around bend testing jigs, transverse to the weld axis. Weld faces and roots are held in tension during face and root bend testing. When evaluating thick plates, the weld cross section is typically bent in tension. Welder performance tests and welding techniques use it the most frequently. Testing of this kind is quite effective at finding liner fusion flaws, which frequently show up on the plate surface. These guided bend tests are used to evaluate the weld metal at the joint's face and root. They evaluate the efficiency, penetration, and fusion of the weld. Testing of this kind can be jigged. The welded plates are used to create the test specimens. These specimens ought to be able to be bent using our bending jig. The test sample is positioned on the die support, which is the base of the jig. The specimen was pushed inside by the hydraulic jack's plunger, which displayed the die shape. The resistance to localised shift indentation is the definition of hardness. We can refer to resistance to wear, abrasion, and indentation. This non-destructive test is hardly ever utilised in the real world, though. As the necessary hardness is attained, the hardness test is used to regulate the qualities of the material. The test establishes the hardness of the weld metal. Determine the impact of welding heat on the base metal's fundamental qualities by closely inspecting the weld joint.

1.11 WELDING DEFECTS

When welding methods or welding patterns are used incorrectly, imperfections in the weld metal result. The weld bead's fault might not be of the desired shape, size, or quality. Defects may appear on the outside or interior of the weld metal. If a fault is within acceptable bounds, such as a fracture, it may be allowed. The most dreaded welding fault is the weld crack. These might appear on the surface, within the weld material, or in areas that have been exposed to heat. When weld joints crystallise, hot crack happens because the temperature might reach over 10,000°C. At the conclusion of welding, when the temperature is very low, cold cracks appear. After welding, a cold fracture may develop hours or days later. Undercut: A notch-shaped groove develops when the metal base melts away from the weld zone. It lessens joint strength exhaustion. Spatter is the term for metal flakes that emerge from a weld and remain on the surface. When gas or tiny bubbles become trapped in the welded zone, porosity develops. When the weld face extends past the weld toe, a fault results. The metal used for the weld rolls and creates a less than 90-degree angle. The outside edges cool more quickly than the crater because the crater does not completely fill up before the arc breaks. As a result, there is stress and a crack. Slag inclusion: Slag in the weld decreases the metal's ability to weld and the material's toughness. Due to this, the weld's structural performance is reduced. Slag can accumulate between welding turns or on the weld surface. The metal pre-solidifies when the welder incorrectly welds the material, leaving a gap that is not filled with molten metal. This results in incomplete fusion. Spatter is the result of metal drops expelled from the weld sticking to the nearby surfaces. By improving the welding environment, scatter can be lessened and then eliminated through grinding. Visual examination, radiographic testing, and tensile tests have all been carried out in the current study. The microstructure of the weldment has also been studied in order to assess the weld's quality. Figure 1.3 displays the photographic perspective of a few welding flaws.

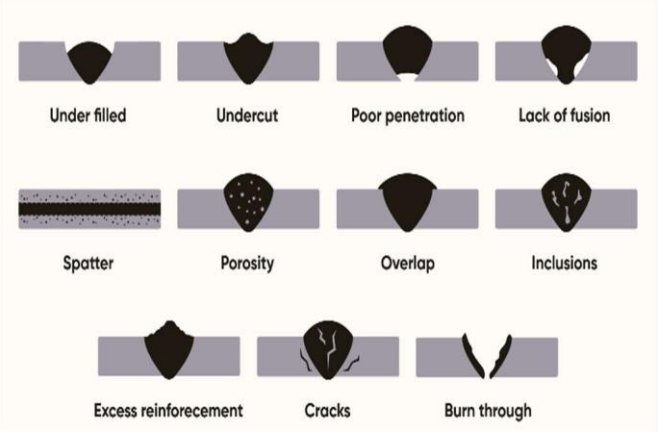

Fig.1.3 TIG Welding defects

Chapter 2

LITERATURE REVIEW, SCOPE AND OBJECTIVE OF PRESENT WORK

2.1 LITERATURE REVIEW

Ramkumar et. al [1] showed TIG welding was used to test the weldability of AISI 430 ferrite stainless-steels both with and without active fluxes. In this study, SiO_2 and Fe_2O_3 fluxes were used to compare the mechanical, metallurgical, and depth of penetration of AISI 430 weld beads. Vora and Badheka [2] comparatively studied on reduced activation ferritic-martensitic (RAFM) steel plate of 6 mm thickness and find the effect of single and double post- weld heat treatment cycles on mechanical property of the joints.

Rajput et. al [3] in their study, same and different junctions on AISI 316L and AISI 409M were evaluated utilising MIG welding at varying notch angle root spacing. The strength of welding joints that were similar and different was compared using tensile testing. The joining arrangement is shown to have an impact on the mechanical characteristics and interfacial microstructure. Yield and tensile strength of root gaps of 2 mm with 60° notch angles were found to be high for comparable welding and at their highest for dissimilar butt-welding connections.

Vidyarthy, Dwivedi and Vasudevan [4] explored utilizing SUPERTIG ER 309L as a filler in A- TIG and M- TIG welding a plate of 8mm thickness of grade AISI 409 ferritic stainless-steel. Furthermore, evaluations were on the basis of mechanical and metallurgical characteristics. To achieve full pentation, bead on plate welding was done utilizing various combinations of flux coating density, welding current, and welding speed. As a result, the 409 FSS weldment's mechanical strength and joint penetration can both be increased by using the A-TIG method.

Raveendra et. al [5] found that the study was performed to compare the effects of pulsed and non-pulsed current on the properties of weldments made of 3mm thick AISI 304 stainless steel using GTAW procedures. Because to fine grain refinement caused by heat exposure, maximum hardness is found there. The non-pulsed current weldments have the highest tensile strength. It was also seen that non-pulsed

current weldments had greater ultimate tensile strength (UTS) and yield strength (YS) values than the parent metal and pulsed current weldments.

The TIG welding on 718 Nickel based super alloy of 2.5 mm thick plate. The welding processes performed at range of welding current 44-115 A, voltage 13-15 V and welding speed of 67 mm/min. Siva-prasad and Raman [6] studied TIG weld fatigue characteristics under two heat treatment conditions. Roy et. al [7] investigated heat treatment effects on TIG weld joints of AISI 304L 3 mm thick stainless steel. The welding was performed on low, medium and high heat condition. Greater tensile strength, percentage of elongation, and microhardness are more influenced by medium heat input.

Ghosh et. al [8] in order to examine dissimilar welding on AISI 409 ferritic stainless steel and AISI 316L austenitic stainless steel, gas metal arc welding with 316L filler wire was utilised. Using a Taguchi L9 orthogonal array, the experiment was conducted. Examining the weld's yield strength, tensile strength, and percentage of elongation.

Anttila et. al [9] investigated gas metal are welding of low and medium chromium ferrite stainless steel utilising various filler wires. To distinguish between the joints, tensile strength, impact toughness, microhardness, and Erichsen cupping tests were conducted. The effects of post-weld heat treatments on ductility and toughness were examined.

Lothongkum et. al [10] conducted TIG welding on 3mm thick AISI 316L stainless steel plates in various positions. It uses pure argon as a shielding gas. With the aid of welding speed and nitrogen concentrations in argon shielding gas, a satisfactory weld bead profile with complete depth of penetration was examined. According to the findings, increasing the nitrogen component in argon gas reduces the pulse currents and speeds up welding.

Vidyarthy and Dwivedi [11] A- TIG welding was used to examine the corrosion behaviour of AISI 409 ferritic stainless steel that is 8 mm thick. With a welding current of 215 A, a flux coating density of 0.81 mg/cm^2, and a welding speed of 95 mm/min, the largest and least corrosion were discovered, respectively. With a welding current of 190 A, a flux coating density of 1.40 mg/cm^2, and a welding speed of 120 mm/min.

Ambade et. al [12] studied tri-component oxide flux on weldability of Inconel 718 welding joints. The results of the joints show that mixing of flux remarkably increases depth of penetration compared to conventional TIG welding. Vidyarthy and Dwivedi [13] investigated weldability of AISI 409 steel using

A-TIG welding process. They have demonstrated how several elements, such as activation flux and its effect on bead geometry, can interconnect.

Ambade et. al [14] explored that the many welding techniques used to join AISI 409M SS, including TIG, MIG, and SMAW. Goldak heat source model's comparison of experimental results and simulation results. The computational and experimental results for those welding processes have, in the end, been found to be outstanding.

Lakshminarayanan et. al [15] investigated the effects of welding with SMAW, GMAW, and GTAW on the tensile and impact properties of 4 mm thick AISI 409M ferritic stainless steel. They found that GTAW weld joints of AISI 409M FSS have better tensile and impact performances than SMAW and GMAW joints because the fusion and HAZ zones include fine grain structure.

Narang et. al [16] found that TIG welding process simulation using fuzzy logic was examined. The TIG welding of steel plates with varying thicknesses under various conditions, such as a welding current range of 55-95 A and a welding speed of 15-45 mm/sec. to prophesy the characteristics of the depth of penetration, shape profile, and bead reinforcement macrostructure zones.

Gupta et. al [17] studied how different heat inputs affected the microstructure and mechanical characteristics of 409L ferritic stainless steel when gas metal arc welding with ER304L and ER308L as two different austenitic filler wires. In this study, heat input values of 0.3, 0.4, and 0.5 kJ/mm were employed. It was found that the microstructure, microhardness, tensile characteristics, microstructure percentage dilution, and chromium nickel ratio were all impacted by the heat input. The mechanical characteristics of welded samples with a heat input of 0.4 kJ/mm are exceptional.

Köse and Topal [18] studied Plasma arc welding (PAW) have been performed of ferritic stainless steel AISI 410S using different welding currents condition. Post-weld heat treatment was used to evaluate the differences in mechanical characteristics and microstructure between PWHT cases and those without PWHT. As a result of the tensile test, all samples also experienced ductile fracture modes.

Amuda and Mridha [19] performed welded joints of ferritic stainless steel AISI 430 using TIG welding technique with energy input ranging from 0.205 to 2.05kj/mm and is then examined for microstructure and hardness. According to the microstructural examination of the welds with varying heat input rates, the fusion zone and high-angle zone, respectively, are expected to contain the inter dendritic martensite and grain boundary martensite, along with certain inter metallics in variable proportions. According to the

hardness values measured across the welds, when more heat is supplied during welding, grain refinement and intermetallic presence are decreased, allowing transformation to take place inside the dual phase zones.

Pasupulla et. al [20] analysing the mechanical behaviours of a welded joint and the flaws generated by these mechanical behaviours, such as destructive testing performed on a work piece during tensile, bending, hardness, and impact testing. TIG welding equipment is used to create the inner flaws of the sample that were discovered by non-destructive radiography testing on stainless steel 304(SS304) plates. After completing the assignment, compare mechanical flaws and radiographic testing flaws with the quality and functionality of the TIG-welded plates. the sample's internal flaws were discovered by radiographic testing. Finally, they compared mechanical flaws and flaws discovered during radiographic testing to the performance and quality of the TIG-welded plates.

Yan et. al [21] studied the microstructure and mechanical properties of laser, tungsten inert gas (TIG), and hybrid laser-TIG junctions made of 304 stainless steels. Microscopy was used to look into the characteristics of joints' microstructure, and X-ray diffraction was used to look into the phase composition. After that, the fracture surfaces underwent tensile tests. The results show that among all joints, the laser-welded junction had the highest tensile strength and the smallest dendritic size, whereas the TIG-welded joint had the lowest tensile strength and the largest dendrite size, with transition zones and heat-affected zones visible in the TIG joint. The fractography observation revealed that the TIG welding joint exhibited a cup-cone-shaped fracture, but the laser welding and hybrid welding joints showed pure-shear fractures. Laser and hybrid welding are both suitable for connecting 304 stainless steels due to their rapid welding times and outstanding mechanical properties.

Durgutlu [22] evaluated the microstructure, depth of penetration, and mechanical properties of 316L during TIG welding while using various shielding gas compositions. Higher mean grain size, penetration depth, and width of 316L austenitic stainless steel were achieved by using hydrogen in argon as a shielding gas, leading to higher tensile strength.

Aslam and Sahoo [23] evaluated the effects of gas metal arc welding on a mild steel substrate covered with stainless steel AISI 304 (GMAW). Microscopical and EDS tests confirm the effective deposition, and a computer model has been developed to assess how welding conditions affect the profile of the clad beads. The results showed that non-uniform weld bead formation was observed at lower voltage and low WFR. During cladding at a high wire feed rate.

Kumar and Shahi [24] investigated joints manufactured of 304 stainless steels (SS) were looked at for their mechanical and metallurgical qualities in relation to heat input. The researchers came to the conclusion that welding joints with low heat input had higher ultimate tensile strength (UTS) than joints with medium and high heat input. The average dendrite length and inter-dendritic spacing increased as the heat input increased, and the heat impacted zone (HAZ) revealed considerable grain coarsening. In gas tungsten arc welded ferritic stainless-steel joints, the impact of filler metals on fatigue crack growth behaviour was examined by Shanmugam et. al [25] Because of its increased yield strength, hardness, and toughness, duplex stainless steel filler metal has been observed to have better fatigue performance.

Mahajan et. al [26] In relation to the make-up of the filler material, the welding characteristics of stainless steel 304 when it is joined using a semi-automatic TIG method were explored. 6 mm thick plates and single V-butt joints were utilised for this. Then, utilising various filler materials including ER 308L, 316L, and 310, the surface roughness, tensile strength, hardness, and EDAX/SEM analysis of the joints were carried out and evaluated. The filler materials ER 316L and 310 have fewer desirable qualities when compared to ER 308L. By using SEM/EDAX analysis, high alloying components were discovered in the joints created using the filler materials ER 310, ER 316L, and ER 308L. It was also demonstrated that joints made using ER 316L filler material resulted in high alloying components.

Wang et al. [27] explains the effects of TIG arc welding parameters on the morphology, microstructure, tensile property, and fracture of welded joints. The tensile strength, yield strength, and elongation of the welded joint all increase initially before declining when the welding current is increased. With a reduction in welding speed and an increase in welding current, the heat input rises. It may cause the welding pool to broaden and deepen, the number of columnar crystals in the seam to decline, and the number of free dendritic crystals to rise. The strength and elongation may decrease with an increase in impulse frequency. The tension fracture is ductile, and the dimples disperse across the fracture surface. The microstructure and tensile properties combine to optimize process parameters, with welding current, speed, and impulse frequency.

In Gas Tungsten Arc Welding (GTAW) of dissimilar metals, Kumar and Mittal [28] investigated the effects of welding parameters such as welding current, gas flow rate, welding speed, electrode, etc. as inputs that affect the outputs like tensile strength and weld hardness.

Zhou et.al [29] studied how the filler material's composition affected the stainless steel 304's welding properties when it was welded utilising a semi-automatic TIG process. Particularly, single V-butt joints

and 6 mm thick plates were employed. Then, the surface roughness, tensile strength, hardness, and EDAX/SEM analysis of joints were assessed using a variety of filler materials, including ER 308L, 316L, and 310. The filler materials ER 316L and 310 displayed less desirable qualities as compared to ER 308L. According to SEM/EDAX analysis, the joints created using the filler materials ER 310, ER 316L, and ER 308L included high alloying components. Another discovery was the production of high alloying components in joints created using ER 316L as a filler material.

Vidyarthy and Dwivedi [30] studied the corrosion behaviour of the A-TIG weld fusion zone is a problem, however AISI 409 ferritic stainless steel is employed in freight train carriages, ocean containers, and equipment for sugar refineries. For the purpose of analysing the corrosion behaviour, potentiodynamic polarisation tests were run.

Mousazadeh and Haghighi [31] investigated inter-pass temperature has an impact on the microstructure growth and mechanical characteristics of AISI 430 when it is autogenously tungsten inert gas (TIG) welded, leading to a higher amount of martensite and a larger HAZ width and grain growth, which results in low tensile strength and ductility.

Lakshminarayanan et. al [32] examined the mechanical properties and microstructure of ferritic stainless-steel joints made with AISI 409M grade by electron beam welding. Results showed that the base metal and weld metal are overmatched, but the joints showed respectable qualities for impact toughness and bend strength.

Akita et. al [33] studied Ferritic stainless steel SUS430 welds with various filler metals for joint microstructures, mechanical characteristics, and fatigue behaviour. The MIG butt welding of SUS430 had involved the employment of two filler metals, Filler I and II, with differing chemical make-ups. In Filler I, Al and Ti were among the coarser grains that could be seen in the microstructure. Due to the production of martensite, which is a hard material that resembles a needle, the heat affected zone (HAZ) in both welded joints had the highest hardness. The filler I welded joint required more heat to weld than the filler II welded joint. Because of this, Filler I's martensite content was both larger and more numerous than Filler II's.

Mohandas et. al [34] ferritic stainless steel that complies with AISI 430 was studied to determine the effects of the welding process shielding gas and the addition of grain refining components on the tensile parameters of the weld zone. Gas tungsten arc welds with equi-axed grain morphology had greater tensile

and yield strengths than shielded metal arc welds. In comparison to shielded metal arc welds, gas tungsten arc welds also had a slightly greater average tensile ductility. Welds typically showed low ductility in relation to the base metal. The addition of copper and titanium boosted the alloy's strength in comparison to the original alloy. The observed properties may be related to the austenite concentration and fracture morphology.

Lakshminarayanan and Balasubramanian et. al [35] in their studied showed that Friction stir welded joint made of ferritic stainless steel 409M was examined for microstructure and mechanical characteristics. At a welding speed of 50 mm/min and a rotation speed of 1000 rpm, flawless single pass welds without volumetric flaws were created. Transverse tensile, impact, bend, and microhardness testing were all carried out. Due to the fast-cooling rate and high strain created by severe plastic deformation brought on by frictional stirring, the base material's coarse ferrite grains are transformed into very fine grains with a duplex structure of ferrite and martensite. According to tensile tests, the base metal and weld metal are overmatched. Acceptable ductility and impact toughness are also displayed by the joints.

Friction stir welding was applied to a plate of 4-mm-thickness of grade AISI 409M ferritic stainless-steel, with empirical relationships established between process parameters and mechanical properties by Lakshminarayanan and Balasubramanian et. al [36].

Dinaharan et. al [37] in their investigation, it was found that 4 mm thick AISI 409 ferritic stainless-steel tubes were MIAB weldable. MIAB welding is utilised in industries to link metallic tubes and pipes. The joint region grew larger as the arc rotation current increased, and the axial shortening increased as well. At higher and lower current limits, the upsetting was incorrect. Due to grain refinement and dislocation fields, TMAZ demonstrated a multifield improvement in hardness, and the selection of arc rotation current is essential to achieving sound joints.

A ferritic stainless steel was joined utilising Gas Tungsten Arc Welding both with and without filler metal, as well as with filler metal that is typically austenitic stainless steel (GTAW). In the heat affected zone, microstructure showed martensite laths and a coarse ferritic matrix (HAZ). Austenite, martensite, and ferrite were shown to be associated with dilution between the filler and base metal Delgado et. al [39].

Zaman et. al [40] investigated that AISI 430 butt TIG welding. The investigations show the existence of martensites and carbides in the grain boundaries together with coarse grain structure in HAZ and FZ. FSS

has limited ductility and is vulnerable to cracking in stressful environments because of its greater strength and hardness at the weld zone.

Delgado et. al [41] experimented to combine a ferritic stainless steel, the Gas Tungsten Arc Welding process was used to conduct both welds without filler metal and welds utilising a typical austenitic stainless steel filler metal (GTAW). The Heat Affected Zone's microstructure in the Heat Affected Zone showed a coarse ferritic matrix and martensite laths (HAZ). When austenite, martensite, and ferrite were present in the weld metal, there was dilution between the filler and base metal. While ductility was 25% higher than base metal, improving toughness, tensile strength increased.

Ghosh et. al [42] studied ferritic stainless steel weld specimens were subjected to an X-ray radiography test to look for surface and sub-surface flaws. Yield strength, ultimate tensile strength, and the percentage of elongation of the welded specimens have all been used to assess the weld's quality. By evaluating ultimate tensile strength, yield strength, and % elongation in addition to the use of Grey-Tag, the observed data have been evaluated, discussed, and analysed.

MIG welding has been used to join samples of AISI 316L stainless steel in butt joints with various settings investigated by Ghosh et. al [43]. The effects of the process parameters have been evaluated using both visual inspection and X-ray radiographic examinations. The weld's quality has been evaluated in terms of ultimate strength, yield strength, and percentage of elongation.

Ghosh et. al [44] experimented and studied, the impact of current, gas flow rate, and nozzle to plate distance on the weld quality of AISI 316L austenitic stainless steel during metal inter gas arc welding has been investigated. Ibrahim et. al [45] This study examined the effects of various parameters on welding penetration, microstructural analysis, and hardness measurement in mild steel. The explored GMAW technique is a pioneer in the development of arc welding.

Karadeniz [46] investigated on welding penetration in Erdemir 6842 steel plate of 2.5 mm thickness was examined in relation to various welding conditions. In contrast to arc voltage, which had a less significant impact, it was discovered that increasing welding current enhanced the depth of penetration.

Kim et. al [47] studied MATLAB/SIMULINK software to choose the best welding parameters based on multiple regressions and a neural network, this paper creates an intelligent system for GMA welding operations. Sharma et. al [48] investigated that weld bead geometry has a significant impact on the welded joint's mechanical strength and quality, and is dependent on the input parameters values.

Narang et. al [49] showed that Butt joint welding was carried out in order to predict the characteristics of the weld bead geometry. The mathematical equation was created using the Taguchi statistical method, and the ANOVA test was used to determine whether the developed equation was sufficient. By choosing the proper process parameters values as specified by the developed models, weld bead geometry can be predicted with accuracy.

Kumar and Shing [50] investigated the impact of oxide flux on weld form, microstructure, and mechanical properties in 304 austenitic stainless steel welded joints using six different types of oxides: Cr2O3, FeO, Fe2O3, MoO3, SiO2, and Al2O3. 8mm thick austenitic stainless-steel plate was joined by autogenous TIG welding, and a thin oxide layer was added before welding. Although Al2O3 performed poorly, the results showed that employing metal oxides significantly increased penetration depth. When several oxides were applied, distinct microstructures were discovered. Both the original metal and the weld had essentially identical mechanical characteristics.

2.2 SCOPE AND OBJECTIVE OF THE PRESENT WORK

With this knowledge, it is obvious that a variety of process control factors, such as welding current, voltage, and gas flow rate in TIG welding (commonly known as TIG welding), can directly or indirectly affect a wide range of quality aspects of the weldment. Weld quality, which is well known to be dependent on bead geometry and mechanical-metallurgical properties of the weld, is expected to be significantly impacted by input parameters including current, voltage, electrode stick-out, gas flow rate, edge preparation, welding position, and welding speed. These quality indices define how much joint strength is necessary to meet the functional requirements of a certain weld, which is more significant for welds in real use. As a result, creating a high-quality weld seems to be a challenging task. According to a review of the published literature, some research has been done on the effects of these factors on weld bead shape and microstructure, as well as other aspects of TIG welding. Among other factors, the final weldment's quality might be affected by the filler metal utilised. A examination of the literature revealed that the mechanical and metallurgical characteristics of welds have not been adequately investigated. One of the areas where more extensive research significantly helps to the exact control of welding procedure for enhanced and acceptable weldment quality is stainless austenitic steel welding, and TIG welding in particular. More research is needed to gain a better knowledge of the different aspects of TIG welding. Analytical analysis, modelling, and experimentation can all be used to investigate how different results are impacted by different process parameters.

There are several tools available for modelling process responses utilising multiple linear regression and response surface techniques. Each quality attribute is optimised (maximised or minimised) in line with the demand to determine the most efficient configuration of the parameters. On the other hand, this tactic can be applied to enhance a single aim function. It is crucial to combine many objectives into a single objective function that must then be optimised when the procedure is complete. The Taguchi method has been shown to be successful in numerous investigations. The results of this method are based on OA design, the quadratic quality of replies idea, and a small number of well-balanced tests. The conventional Taguchi method cannot be used to tackle a multi-objective optimisation problem. To counter this, the Taguchi method and grey relational analysis will be applied. The impact of various processes/input parameters on the quality of weld in austenitic stainless steels when utilising TIG welding still needs further study, despite the fact that there has been a lot of research on many aspects of welding. There are numerous input parameters/features when TIG welding austenitic stainless steels that can impact the weldment's quality.

Other input features exist in addition to current, gas flow rate, voltage, welding speed, electrode stick-out, and the type of inert gas or gas mixture. When preparing the edge for welding, elements such as filler rod composition and diameter, power source specifications, welding location, etc. should be taken into account. It will take a lot of research to determine how these traits or variables affect the weld's quality. Austenitic steel TIG welding requires significant experimentation, analysis, and modelling in order to better understand the phenomena, manage process parameters, optimise the process parametrically, and forecast and control desired outcomes (quality indices). A knowledge foundation that engineers and workers in the field may utilise to make high-quality welds with increased accuracy, dependability, and foresight has been developed as a result of several investigations. In order to ascertain how these parameters, affect the quality of the weld, some of the input features have been considered in this study. These two variables are used in 3mm thick austenitic stainless steel TIG welding: current and gas flow rate. The reaction to a tensile load is evaluated for the ultimate strength and breaking strength of butt-welded joints. The effects of altering the composition of the filler material have also been considered. As a result, this research will examine the current, gas flow rate, and filler material utilised in austenitic stainless steel TIG welding. The results of optical and X-ray radiographic tests have also been used to assess the levels of faults like porosity, lack of fusion, undercut, etc. in addition to the responses in terms of ultimate and breaking strengths. Microstructural studies have also been completed. Regression analysis

and Taguchi-based grey relational analysis can now be utilised to analyse the data using experimental data. Mathematical modelling has also been used to predict how systems will react to changing current and gas flow rates. In order to find the ideal parametric combination for the desired weld quality, the optimisation problem was solved using the Grey-based Taguchi technique. As a result, both the findings of the experiment and the analysis of the data can be used to draw some significant conclusions.

Chapter 3

PLAN, SETUP, AND PROCEDURE FOR EXPERIMENT

3.1 EXPERIMENTAL PLAN

For the present work, butt welding was done 3 mm thick 409M ferritic stainless steel have for this experimentation purpose. The L9 orthogonal array was selected by considering three variables with three levels. The input parameters for this investigation include current, gas flow rate, and travel speed. Nine different butt welds were used to create samples using different current, gas flow rates, and arc gap settings. By doing trial runs and literature research, the levels of the factors are set. Table 3.1 lists the variables and their corresponding concentrations utilised in the experiments. It is listed in Table 3.2 the welding settings that have been almost identical in all nine experiments. The experimental design matrix for each factor is shown in Table 3.3.

Table 3.1 Process parameters and their levels

Process Parameters	Symbols	Unit	Level 1	Level 2	Level 3
Welding Current	C	Ampere (A)	100	110	120
Gas Flow Rate	G	litre/min	10	15	20
Travel Speed	T_s	mm/ min	1	1.5	2

Table 3.2 Fixed welding conditions

Polarity	AC (alternating current)
Arc Voltage	25 V
Electrode Diameter	1.4 mm
Root gap	2 mm
Shielding gas	Argon (99.99%)

Table 3.3 Experimental design matrix as per L_9 orthogonal array

Sample No.	Current	Gas flow rate	Travel speed
1	100	10	1.0
2	100	15	1.5
3	100	20	2.0
4	110	10	1.5
5	110	15	2.0
6	110	20	1.0
7	120	10	2.0
8	120	15	1.0
9	120	20	1.5

The details process parameters of butt-welded joints are shown in Table 3.1. Thus far, this kind of basic experiment has been run. Visual inspection of the welded samples was to be followed by X-ray radiography test, tensile tests, hardness tests, and microstructural examinations.

3.2.1 EXPERIMENTAL SET-UP

This section provides a description of the instruments utilised in the present project.

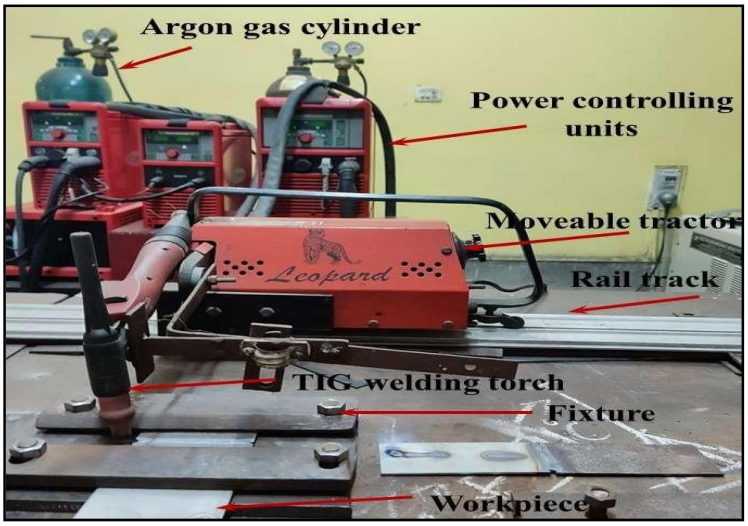

Fig 3.1 TIG welding set-up

3.2.2EQUIPMENTS AND INSTRUMENTS USED

The main set-up of these experiments includes the TIG welding machine.

a) TIG Welding Machine:

This experiment has been performed on Tungsten Inert Gas Welding Machine (Maker: Fronius Magic Wave 2500, India). The photographic views of this setup are shown in the Figure 3.1

SPECIFICATIONS OF TIG MACHINE

Maker:	Fronius Magic Wave 2500, India
Type:	THYRISTORISED
Power supply unit:	3 phase
Torch:	TTA – 200 Straight neck
Shielding gas:	Argon (99.99%)
Type:	Argon LAR 58

b) X-ray radiography machine

SKB Metallurgical Services, Howrah-111062, has performed X-ray radiography tests. The important specifications of this equipment are shown in Table 3.4

Table 3.4 Specifications of the X-ray radiography machine

Equipment details	XXQ-2005
Source	X-ray
Current	5 mV
Voltage	120 kV
Film	LASER NDT-7
Sensitivity	< 2%
SOD	28``
Screen	0.15 mm(both)
Technique	S.W.S.I.
IQI	ASTM-1A
Exposure time	30 Sec
Processing temperature	20°C

c) Milling machine

The required amount of strip is cut from the welded sample using a milling machine to prepare the micro hardness and tensile sample. The specification of the milling machine is given in the Table 3.5 and photographic view of the milling machine used in the work is shown in Figure 3.2.

Table 3.5 Specifications of the Milling machine

Type	Universal Milling Machine
Maker Name	B. S. Machine Tools Corporation
Serial Number	222484

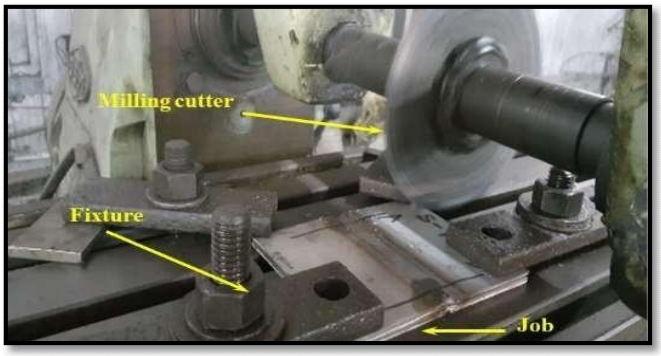

Fig. 3.2 Photographic view of milling machine used in this work

d) Metallurgical microscope:

Leica metallurgical microscope is utilised in the current investigation to examine the microstructures of the welded samples. The specifications are given in Table 3.6. A photographic view of metallurgical microscope is shown in Figure 3.3.

Table 3.6 Specification of the metallurgical microscope

Model	Leica DMILM
Focusing	3 gears focusing
Incident light	sturdy incident light axis with 4x and 5x reflector turrets
Transmitted light	12 V, 100 W halogen
Power supply	90-250 for 12 V 100 W, frequency 50-60 Hz

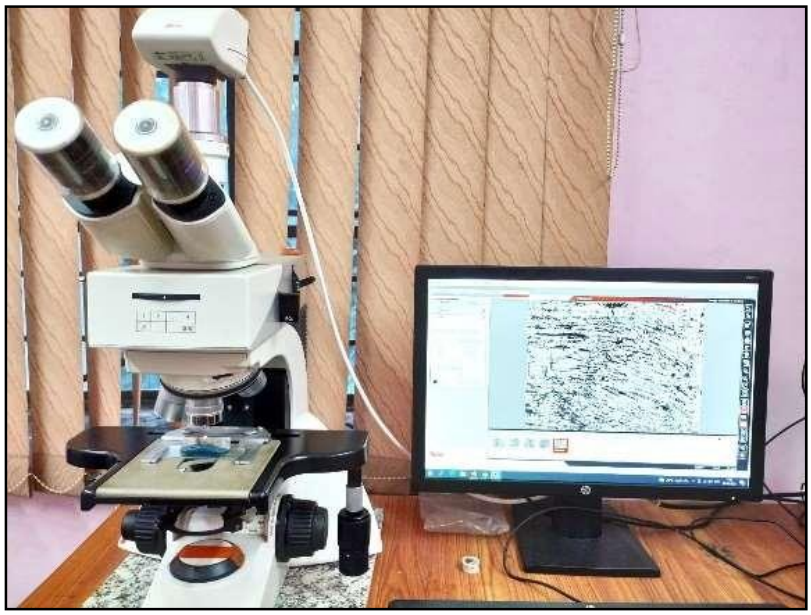

Fig. 3.3 Photographic view of the Leica metallurgical microscope

e) Instron Universal Testing Machine:

Tensile tests were performed at the Department of Atomic Energy's Variable Energy Cyclotron Centre (VECC) laboratory using an Instron universal testing machine. Specimens are secured using a hydraulic chuck, as seen in Figure 3.4. Table 3.7 provides a brief overview of the machine's key characteristics. A picture of the device is also displayed (Figure 3.5).

Table 3.7 Specification of Instron universal testing machine

Model name	INSTRON
Model number	33R 4482
Maximum load capacity	100kN
Maximum speed	500 mm/ min
Maximum force at full speed	75kN
Maximum speed at full force	250 mm/ min
Position measurement accuracy	0.15 %

Fig. 3.4 Hydraulic Chuck

Fig. 3.5 Photographic view of Instron universal testing machine

3.3 COMPOSITION OF THE BASE MATERIAL AND FILLER WIRE

AISI SS 409 M Ferritic stainless-steel sheet are joined in this present work study using the (TIG) tungsten inert gas welding technique. The specimens have dimensions of 100 × 50 ×3 mm. Without any special edge preparation, the samples were cut with a Shearing Machine. Tables 3.8 display the relative compositions of the base materials and filler wires.

Table 3.8 base material's and the filler wire's component compositions

	C	**Mn**	**Si**	**S**	**P**	**Cr**	**Ni**	**Mo**	**Fe**
Base Metal (AISI 409M)	0.08	1.00	1.0	0.05	0.045	11.75	0.5	Bal	Bal.
Filler Metal (ER 308L)	0.030	1.54	0.65	0.030	0.045	19.20	8.68	0.02	Bal.

3.4 EXPERIMENTAL PROCEDURE

In this thesis project, Ferritic stainless steel of grade AISI 409M was exploited. There are a total of 9 welding samples with dimensions of 100 × 60 × 3 mm. The welding set up is tested with the aid of a fixture to make sure it is ready for use. Finally butt joint are made. Nine set welded samples were produced using Taguchi's orthogonal array design of experiments, with welding performed out and at varying current, gas flow rates, and travel speed settings. An image of the fully welded specimen can be found in Figures 3.6 to 3.14.

Fig. 3.6 Photographic view of specimen number S1

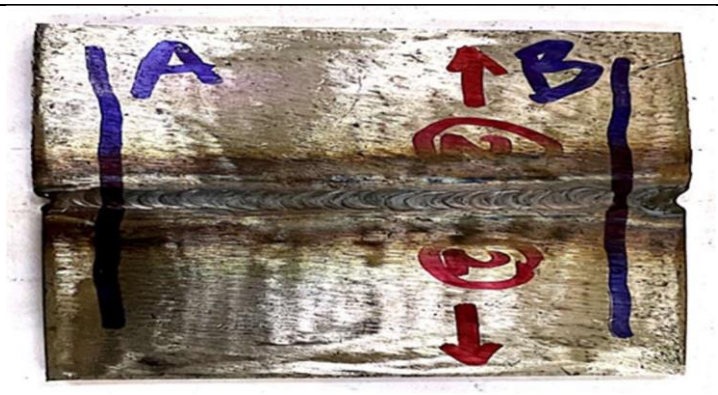

Fig. 3.7 Photographic view of specimen number S2

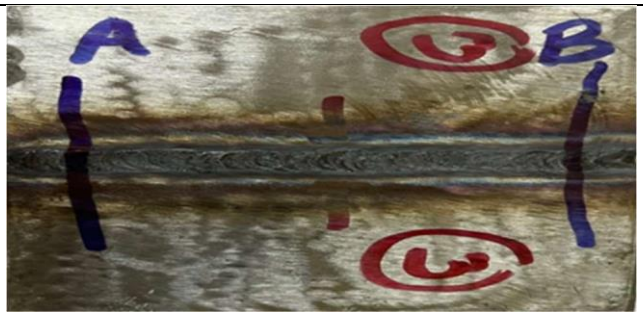

Fig. 3.8 Photographic view of specimen number S3

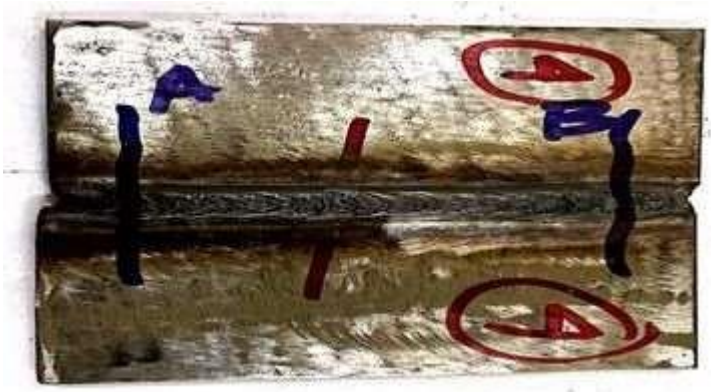

Fig. 3.9 Photographic view of specimen number S4

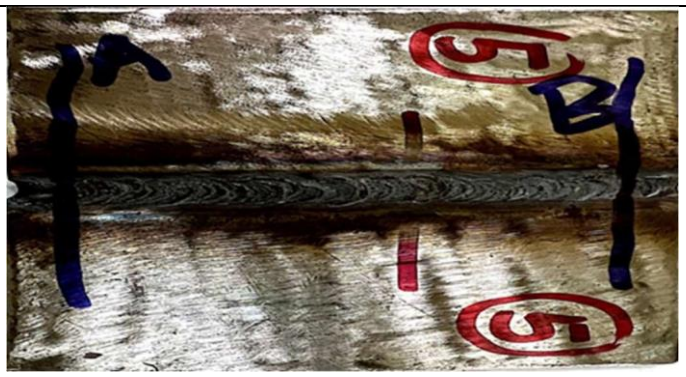

Fig. 3.10 Photographic view of specimen number S5

Fig. 3.11 Photographic view of specimen number S6

Fig. 3.12 Photographic view of specimen number S7

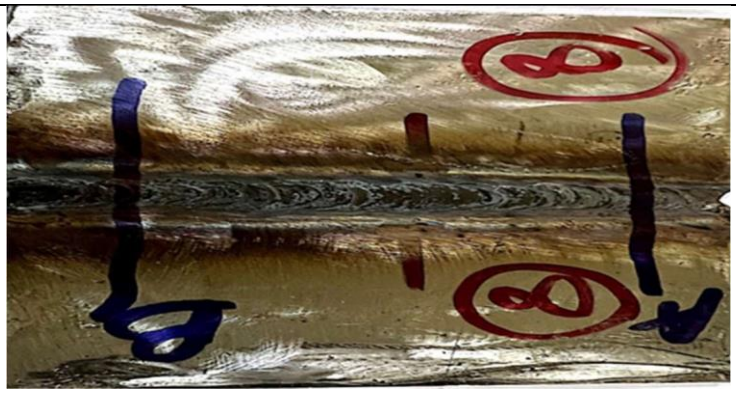

Fig. 3.13 Photographic view of specimen number S8

Fig. 3.14 Photographic view of specimen number S9

The welding samples are cleaned using acetylene, and nine samples were evaluated visually. All welded samples are analysed using X-ray radiography test. A milling machine was used to cut tensile test samples from the weld strip. A photograph of a tensile test specimen is shown in Figures 3.14 to 3.15.

Fig. 3.14 Pictorial view of the tensile test specimen number S1 - S9

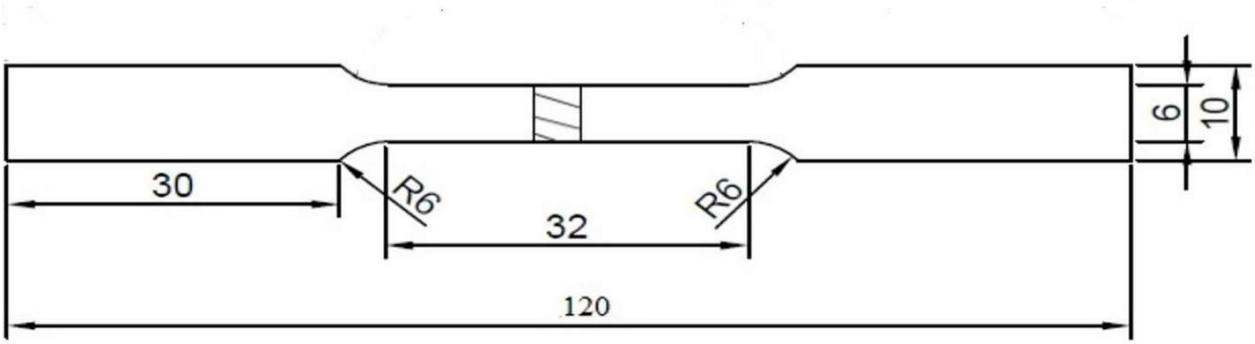

Fig. 3.15: shows the dimensions of the tensile test specimens

A universal testing machine (UTS), which is at the Variable Energy Cyclotron Centre is a premier R & D unit of the Department of Atomic Energy Laboratory at VECC, Kolkata conducts tensile test on the specimens and observation are made. The tensile test specimens' measurements are shown in Figure 3.14. During testing, a hydraulic jaw holds the samples in place. One jaw is fixed and another is movable after increasing the load the specimens are torn out. Small amount of weld region strip cut for microstructural study purpose. After cutting all the specimens are polished using different grade emery paper up to 1800 grade, then the samples are polished by automatic cloth polishing machine and finally etched. Etched composition is aqua regia (3HCl + 1 HNO_3) solution. Under a Leica microscope, samples of base metal (BM), heat-affected zone (HAZ), and weld metal (FZ) were studied. Pictures were also taken. Every one of these samples has also undergone a microhardness test. This technique involved measuring the base metal, the high-hazard zone, and the weld metal's hardness.

Chapter 4

4.1 RESULTS OF VISUAL INSPECTION AND DISCUSSIONS:

Each sample was visually examined once the welding process was finished. The information gathered during the experiment is shown in Table 4.1. Visual flaws in several of the welded samples include undercutting along the welding line and a lack of fusion on the opposite side of the join. Nearly no defects are found in some examples, such as samples 1 and 6, when certain parametric values are used. Environmental factors including voltage fluctuations, the configuration of a semi-automatic equipment, and others can cause errors in some samples. Because the process is manual and human error is easily introduced, the welder's proficiency is essential to the weld's quality. Imperfections or homogeneities in the base metal plates and filler wire might result in weld defects.

Table 4.1: Results of visual inspection

Sl. No	Sample number	Observation
1	S1	No defect
2	S2	Incomplete Penetration
3	S3	Incomplete Penetration
4	S4	No defect
5	S5	Excessive deposition
6	S6	No defect
7	S7	No defect
8	S8	No defect
9	S9	Undercut, Excessive deposition

After welding, austenitic stainless steel weld samples are visually examined for surface defects. The sole method for verifying a large number of welds is visual inspection. Due to its ease, speed, and affordability, this approach is most frequently used to inspect weldments. Table 4.1 lists the findings of the ocular investigation. This table demonstrates that for the given welding settings, no flaws were found. For S1, S4, S6, S7, and S8, respectively. One or more additional samples showed undercutting, blow holes, and splatter. Blow holes could have been generated by low or high current, as well as transit speed. Blow holes or porosity may be caused by an improper welding technique, stringer or woven beads, a dirty work surface, and damp filler rod. Gas trapped in hardening metal, a stronger arc, etc., may have generated blow holes and porosity. Undercuts can be caused by improper welding current, gas flow rate, and nozzle-to-

plate distance. Undercut may be caused by longer arcs, faster arcs, and bad filler rod. The various causes of the sample and X-ray radiography abnormalities are covered in the next section.

4.2 RESULTS OF X-RAY RADIOGRAPHY TEST AND DISCUSSIONS

X-ray radiography tests have been done for all the welding samples after the visual inspection. The results are shown in the Table 4.2.

Table 4.2: Results of X-ray radiography test

Source: X-Ray	Equipment Details: XXO-2005	Voltage: 125 KV		
Density: 2.4-2.8	Sensitivity: < 2% Sensitivity: < 2%	FFD: 28"	Screen: 0.15mm (Both)	
Technique: DWSI	Exposure: 0.8 mins.	Processing Temp./Technique: 20°C/Manual		
SL. NO.	IDENTIFICATION	SEGMENT	FILMSIZE	OBSERVATION
1	S-1	A-B	3"×5"	N.S.I
2	S-2	A-B	3"×5"	Inadequate weld
3	S-3	A-B	3"×5"	N.S.I
4	S-4	A-B	3"×5"	N.S.I
5	S-5	A-B	3"×5"	N.S.I
6	S-6	A-B	3"×5"	Lack of fusion
7	S-7	A-B	3"×5"	N.S.I
8	S-8	A-B	3"×5"	N.S.I
9	S-9	A-B	3"×5"	N.S.I

These results indicate that the majority of samples had enough serious flaws. Defect-free joints have been produced (sample numbers S1–S9) at the appropriate welding conditions. Figures 4.1–4.9 display the schematics used in X-ray radiography.

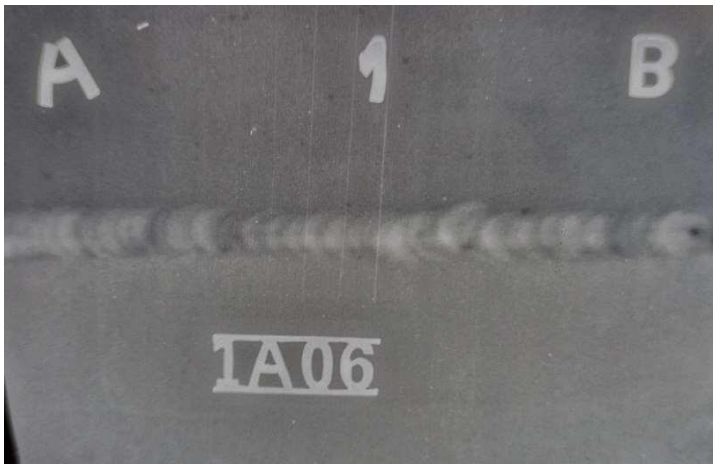

Fig. 4.1 X-ray Radiography film for sample S1

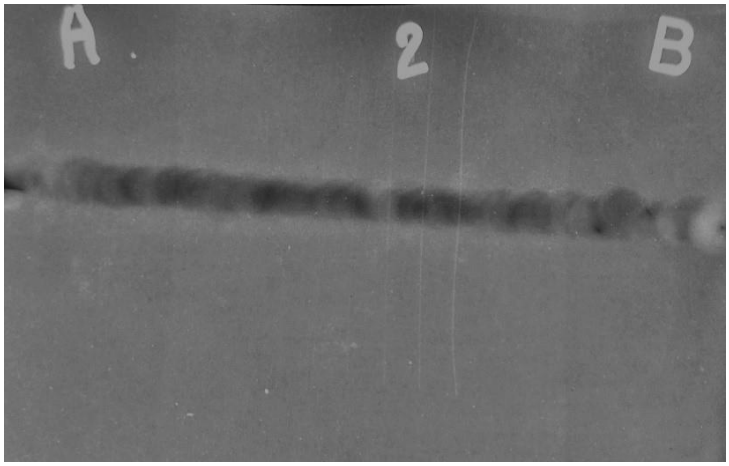

Fig. 4.1 X-ray Radiography film for sample S2

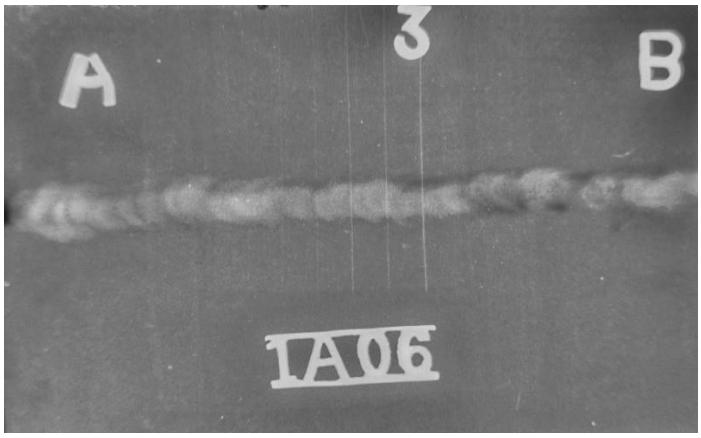

Fig. 4.3 X-ray Radiography film for sample S3

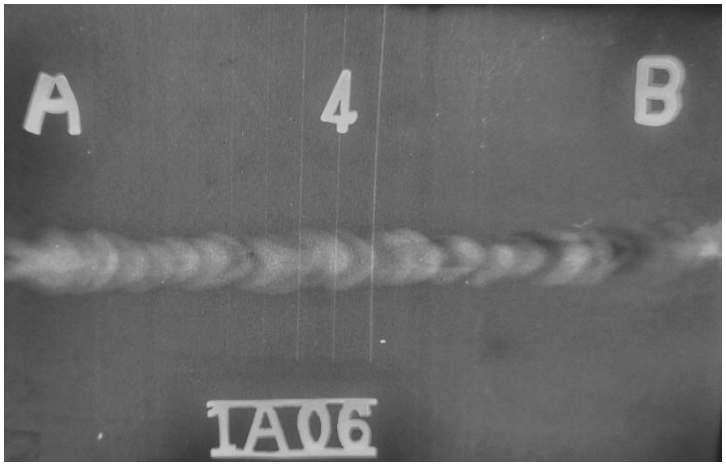

Fig. 4.4 X-ray Radiography film for sample S4

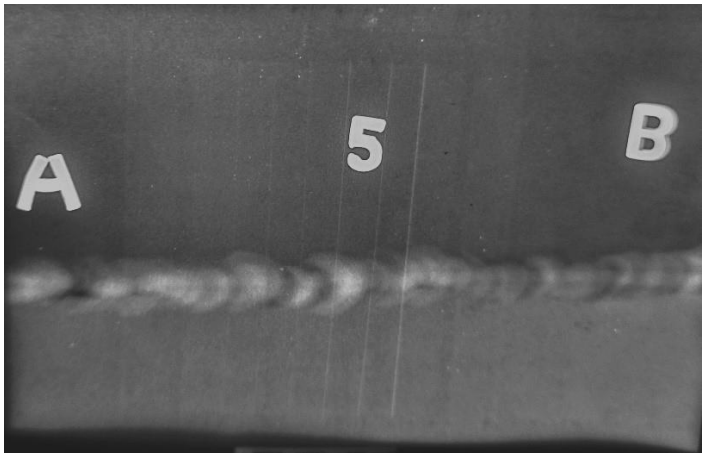

Fig. 4.5 X-ray Radiography film for sample S5

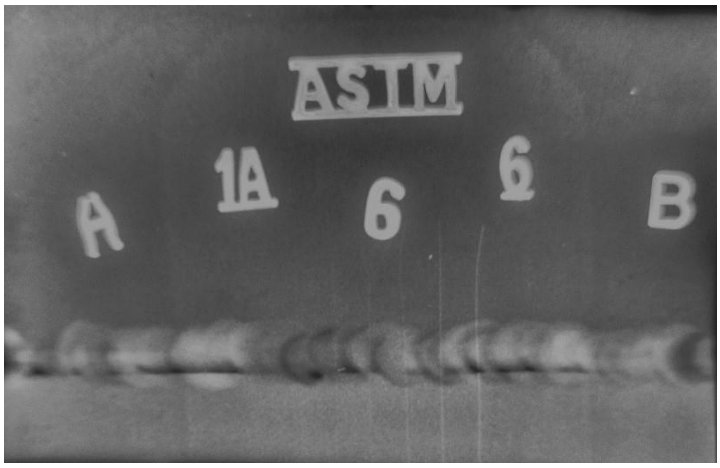

Fig. 4.6 X-ray Radiography film for sample S6

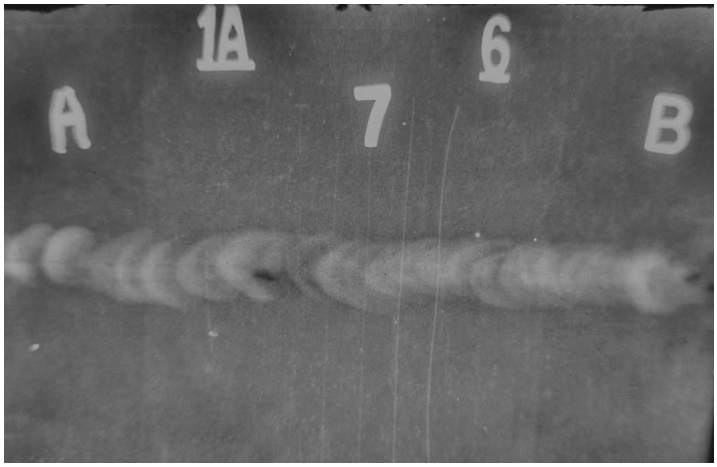

Fig. 4.7 X-ray Radiography film for sample S7

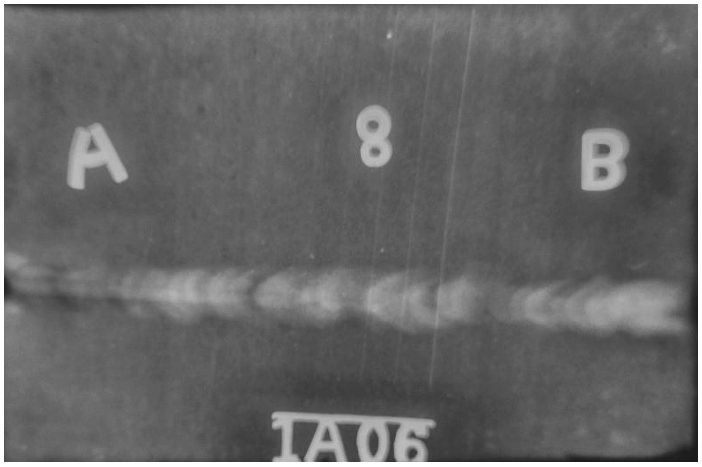

Fig. 4.8 X-ray Radiography film for sample S8

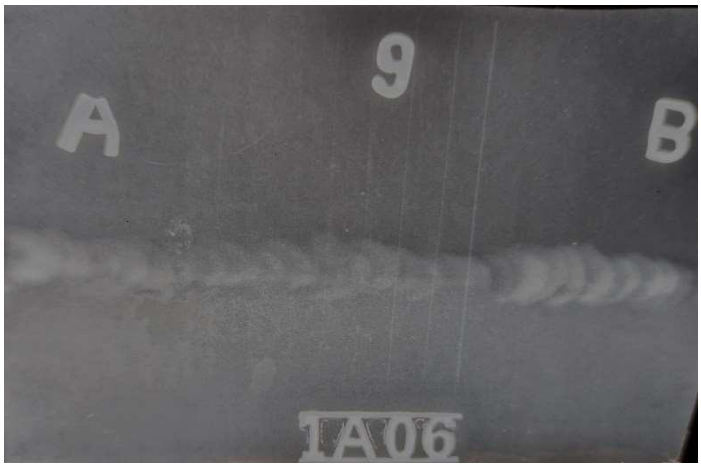

Fig. 4.9 X-ray Radiography film for sample S9

After the visual inspection, all 9 welded samples were subjected to X-ray radiography testing using the X-ray defect detector XXQ-2005. The results of this investigation are outlined in Table 4.2. The photographic views of the X-ray films are shown in Figures 4.1–4.9. A faulty current setting, incorrect cleaning, a faster arc travel speed, the presence of oxides, scale, or other impurities could have prevented the deposited metal from efficiently joining with the base metal. If the heat input is too low, the weld deposit won't melt correctly. Gas entrapment during solidification is one hypothesis for the occurrence of porosity in samples S2 and S6. Porosity can be a major problem that is challenging to resolve.

4.3 RESULTS OF TENSILE TEST AND DISCUSSION

The Instron machine was used to conduct a tensile test in order to look at the areas where failure or fracture occurred and to determine key mechanical characteristics of the welded samples. Table 4.3 provides the results of the tensile testing.

Table 4.3: Tensile test results

Sample number	**Sample Identity**	**Ultimate Tensile Strength (MPa)**	**Elongation percentage (%)**
1	S1	**398.32**	**11.49**
2	S2	542.50	9.47
3	S3	**586.02**	9.39
4	S4	476.57	8.95
5	S5	487.94	8.00
6	S6	457.76	8.35
7	S7	566.89	8.78

8	S8	428.08	11.15
9	S9	464.77	**7.15**

From table 4.3 it reveals that all the butt-welded joints performed satisfactorily and best ultimate tensile strength is obtained for sample number 3, with the maximum value being 568.02 MPa; sample no. S3 having lowest tensile strength of value 398.32. The highest percentageelongation value that has been measured is 11.49% (for sample no. S1). The sample number S9 shows thelowest percentage elongation value (7.15%).

Figures 4.10–4.19 display stress-strain curves that correlate to the tensile test findings of each sample. Nearly all stress-strain curves show typical ductile behavior.

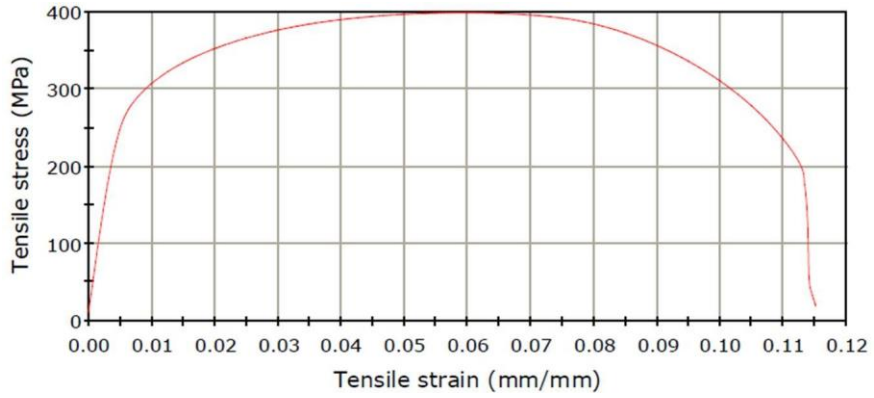

Fig 4.10: Tensile test diagram for sample no. S1

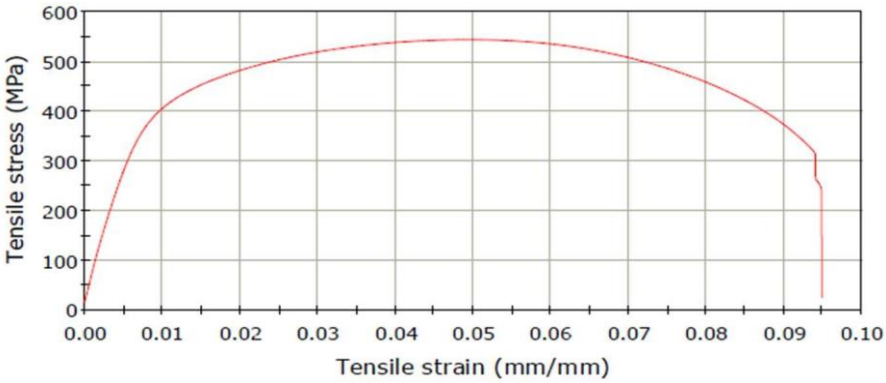

Fig 4.11: Tensile test diagram for sample no. S2

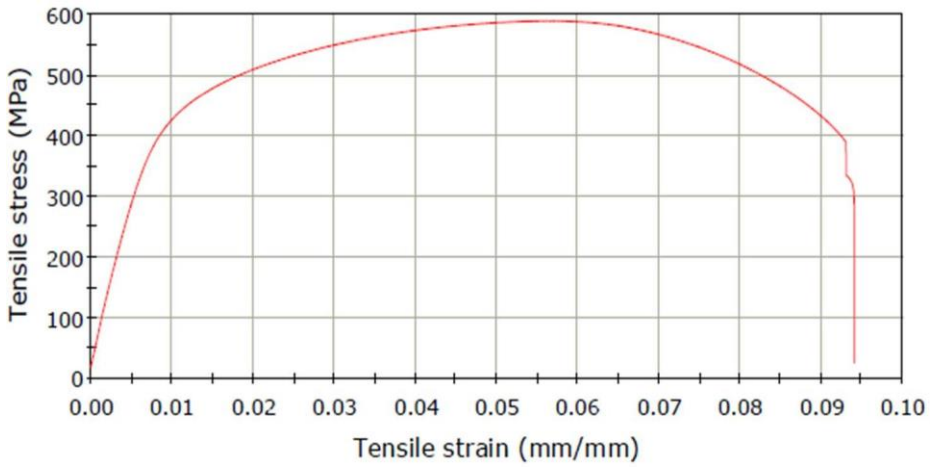

Fig 4.12: Tensile test diagram for sample no. S3

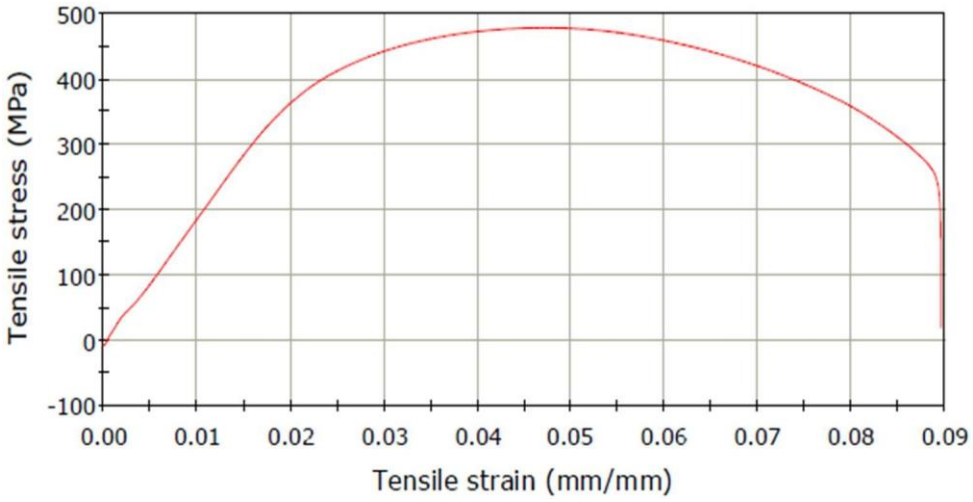

Fig 4.13: Tensile test diagram for sample no. S4

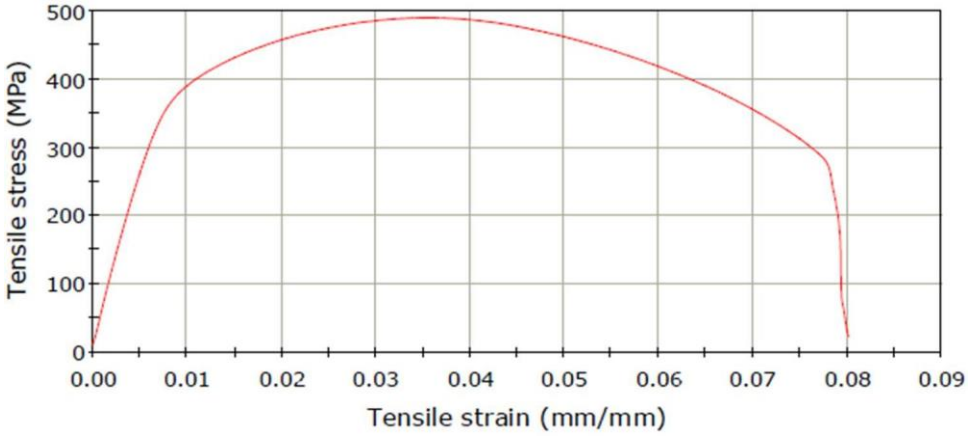

Fig 4.14: Tensile test diagram for sample no. S5

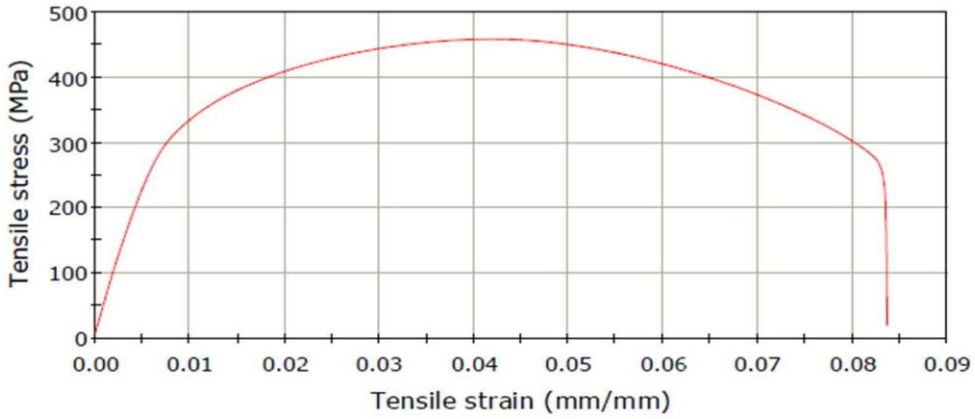

Fig 4.15: Tensile test diagram for sample no. S6

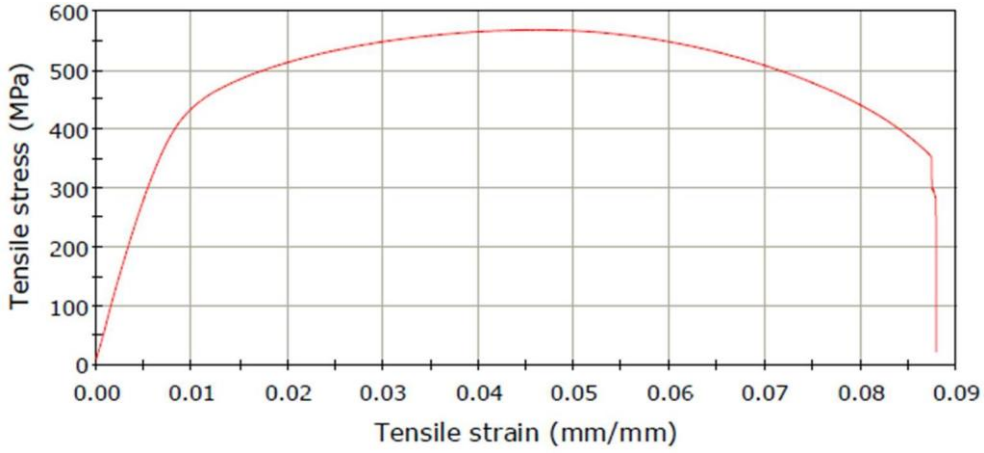

Fig 4.16: Tensile test diagram for sample no. S7

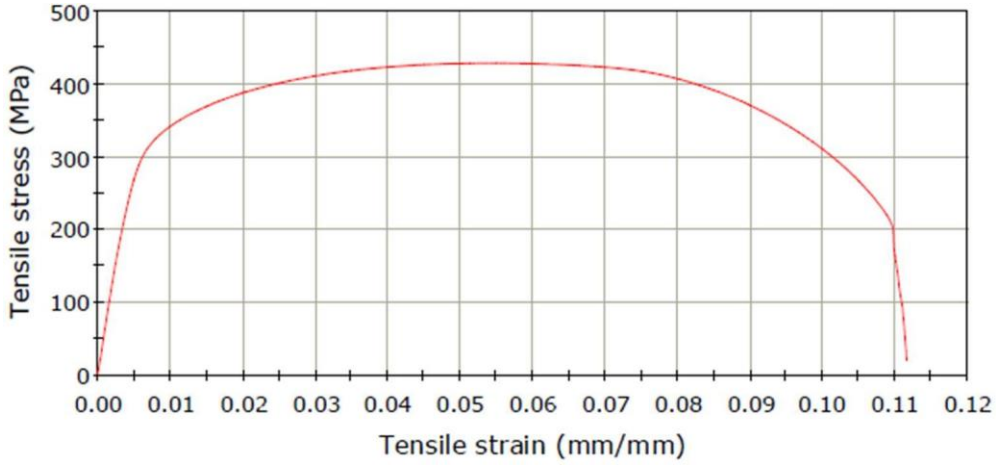

Fig 4.17: Tensile test diagram for sample no. S8

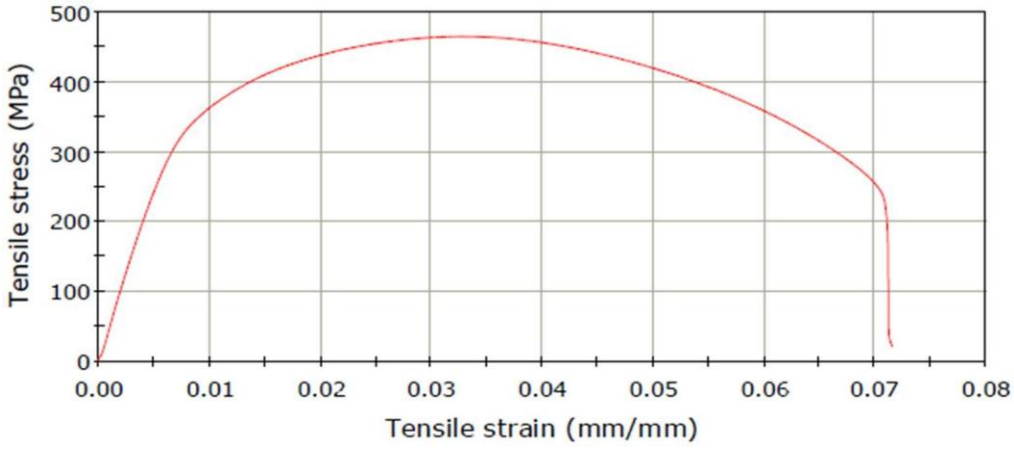

Fig 4.18: Tensile test diagram for sample no. S9

4.4 STUDY OF MICROSTRUCTURES AND DISCUSSION

All of the welded samples have had their microstructures studied, and each sample has had pictures taken in the weld and HAZ regions. The microstructure of base metals has also been researched and Figures 4.19–4.27 depict the microstructures of all the samples.

All samples of the base metal have pure austenitic grains with twin boundaries in terms of microstructure. HAZ microstructures are very similar across nine samples. It is frequently discovered that HAZ microstructures and base metal microstructures are extremely similar. The granules of HAZ, however,are found to be coarser than those of the investigated basic metals. This might be brought on by the HAZ region's slower cooling rate. Results of micro-hardness tests offer proof for the aforementionedclaim. Austenitic twins are present in the HAZ of every sample. Nearly all samples exhibit the presence of -ferrite traces in HAZ. The HAZ area of samples 3 and 9 both includes scattered carbidephases (Figures 4.21 and 4.27, respectively). This sample has the lowest tensile strength. The high tensile test values of samples 1, 2, and 7 (Figures 4.19, 4.20, and 4.25, respectively) were not due to any obvious causes, according to a microstructural analysis of HAZ.

When weld metal's microstructures are compared to those of HAZ and base metal, it is discovered that they are highly unlike from the microstructures of these two materials. The bulk of samples have columnar-dendritic grain growths seen in the weld microstructures. The weld metal, however, can be seen to have equi-axed grain growths in a few samples (samples S4 and S5; Figures 4.22 and 4.23).

Parametric condition change has had an indirect impact on the microstructures of different weldment zones. The effect of altering welding parameters is clear, though. This may be thought about further in depth in the future.

a **b** **c**

Fig. 4.19: Metallographic view of sample number S1(a 100X, b 200X, c 500X)

a **b** **c**

Fig. 4.20: Metallographic view of sample number S2 (a 100X, b 200X, c 500X)

a **b** **c**

Fig. 4.21: Metallographic view of sample number S3 (a 100X, b 200X, c 500X)

a **b** **c**

Fig. 4.22: Metallographic view of sample number S4 (a 100X, b 200X, c 500X)

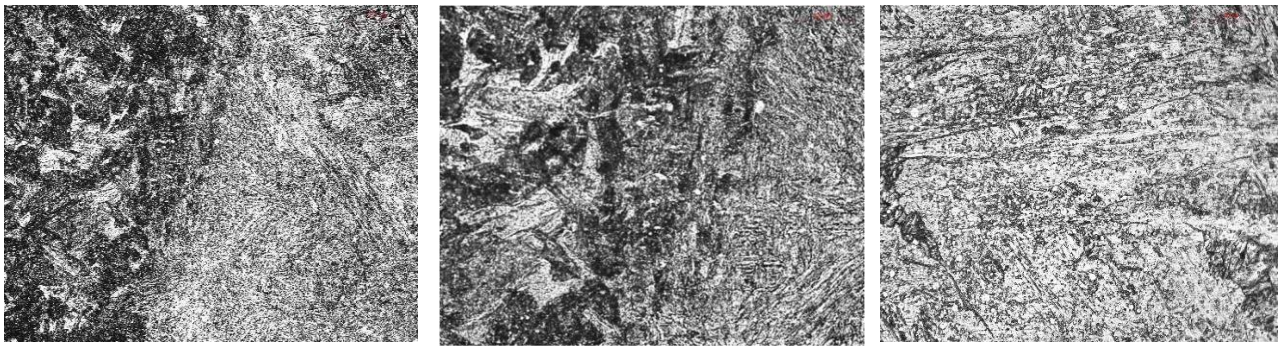

a **b** **c**

Fig. 4.23: Metallographic view of sample number S5 (a 100X, b 200X, c 500X)

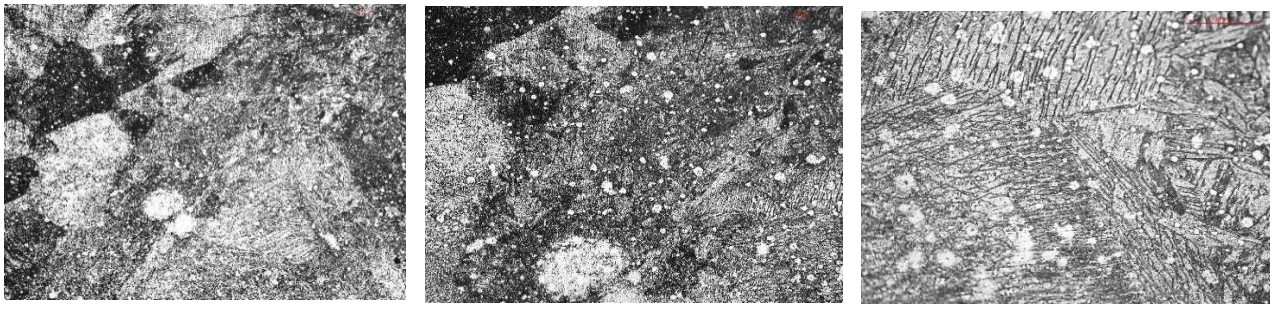

a **b** **c**

Fig. 4.24 Metallographic view of sample number S6 (a 100X, b 200X, c 500X)

a **b** **c**

Fig. 4.25: Metallographic view of sample number S7 (a 100X, b 200X, c 500X)

a **b** **c**

Fig. 4.26: Metallographic view of sample number S8 (a 100X, b 200X, c 500X)

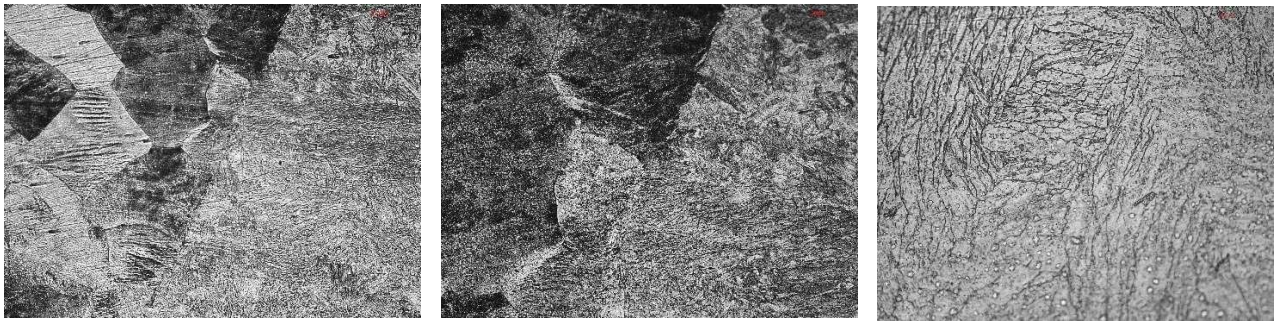

a **b** **c**

Fig 4.27: Metallographic view of sample number S9 (a 100X, b 200X, c 500X)

CHAPTER 5

5.1 TAGUCHI METHOD

The Taguchi technique was developed by Dr. Genichi Taguchi, a Japanese expert in quality management. An effective and systematic strategy for improving designs for performance, quality, and cost is to apply Taguchi quality engineering methods, which employ design of experiments. It is a crucial tool for building high-quality systems at a cheaper cost. The variation of the experiment findings is significantly reduced when the process control parameters are optically set using the Taguchi method, which is based on orthogonal array experiments. An orthogonal array has fewer experiments, but they are more evenly distributed. The best parameter choice for the Taguchi technique, which takes into consideration both the mean and the variability, is assessed using a statistical performance metric known as the signal-to-noise ratio. The method explores the idea of a quadratic loss function. This ratio is calculated by dividing the standard deviation (signal) by the mean (noise). The qualities of the process or product are what determine the ideal ratio. The three most frequently employed standard signal-to-noise ratios (S/N ratios) (HB) are NB, LB, and HB. The parametric combination results in the best S/N ratio. The conventional Taguchi approach cannot be used to tackle multi-objective optimization. The Taguchi method, which is based on grayscale photographs, can be used to achieve this. Deng's grey system theory has been supported by facts ever since it was initially put forth in 1982. The grey relational analysis, which is based on grey system theory, is a useful technique for resolving complex interrelationships among various performance parameters. Experimental data, such as the product's quality attributes, are first normalized so that they range from zero to one in order to do grey relational analysis. The term "grey relational generation" refers to this method. The grey relational coefficient, which is produced using normalized experimental data, is then used to depict the correlation between the desired and actual data. The mean of the grey relational coefficients for a selection of responses is then used to generate the overall grey relational grade. The projected overall grey relational grade affects the multiple response process' overall performance feature. In the same way that it may optimize multiple responses in a process, the objective function can also be used to optimize a single response. The S/N ratio of the entire grey relational grade is then maximized to evaluate it utilizing the Grey-Taguchi approach.

Taguchi's S/N Ratio for (NB) Nominal-the-best

$$\eta = 10\ log_{10}\ \frac{1}{n}\Sigma_{i=1}^{n}\frac{u^2}{\sigma^2} \qquad (5.1)$$

Taguchi's S/N Ratio for (LB) Lower-the-better

$$\eta = -10\ log_{10}\ \frac{1}{n}\Sigma_{i=1}^{n}y_i^2 \qquad (5.2)$$

Taguchi's S/N Ratio for (HB) Higher-the-better

$$\eta = -10\ log_{10}\ \frac{1}{n}\Sigma_{i=1}^{n}\frac{1}{y_i^2} \qquad (5.3)$$

5.2 GREY RELATIONAL ANALYSIS

Experimental data, such as the product's quality attributes, are first normalised so that they range from zero to one in order to do grey relational analysis. The term "grey relational generation" refers to this method. The grey relational coefficient, which is produced using normalised experimental data, is then used to depict the correlation between the desired and actual data. The average of the grey relational coefficients for a group of responses is used to calculate the overall grey relational grade. The decided grey relational grade affects the multiple response process's overall performance feature. The fact that the overall objective function is graded in overall grey relational grades is one of the key benefits of this approach to tackling multi-response optimization problems. The total grey relational grade is used to choose the ideal parametric combination.

The normalized data matching to the Higher-the-Better (LB) criterion in grey relational generation can be represented as follows:

$$X_i(k) = \frac{max y_i\,(k) - y_i\,(k)}{\max y_i\,(k) - min y_i\,(k)} \qquad (5.4)$$

For Higher-the-Better (HB) criterion, the normalized data can be expressed as:

$$X_i(k) = \frac{y_i\,(k) - min y_i\,(k)}{\max y_i\,(k) - min y_i\,(k)} \qquad (5.5)$$

where min y_i (k) is the minimum value of y_i(k) for the kth response, max y_i(k) is the greatest value of y_i (k) for the kth response, and x_i(k) is the value following the grey relational generation. For the responses, x_0(k) is the optimum sequence. The goal of the grey relational grade is to show how closely

related the sequences [x_0(k) and x_i(k), where i=1, 2, 3,..., 16] are to one another. One can compute the grey relation coefficient i(k) as,

$$\xi i(k) = \frac{\Delta \min + \theta \Delta max}{\Delta_{oi}(k) + \theta \Delta max} \qquad (5.6)$$

where $\Delta_{oi} = \|x_0 - x_i(k)\|$ difference of the absolute value x_0(k) and x_i(k); θ is the distinguishing coefficient $0 \leq \theta \leq 1$; $\Delta_{min} = \forall_j^{min} - t\forall k^{min}\|x_0(k) - x_j(k)\|$= the smallest value of Δ_{0i} ; and $\Delta_{max} = \forall_j^{min} - t\forall k^{min}\|x_0(k) - x_j(k)\|$= largest value of Δ_{0i}.

X_i and the comparative sequence X_0 (also called grey relational grade), and $\Delta_{oi}(k)$ is the absolute value of difference between X_0 (k) and X_i (k).

After averaging the grey relation coefficients, the grey relational grade γ_i can be computed as:

$$y_i = \frac{1}{n}\sum_{k1}^{n} \xi i(k) \qquad (5.7)$$

where n is the number of responses to the process. The reference sequence x_0(k) and the provided sequence x_i(k) have an intense relational degree, which is shown by a greater value of grey relational grade. The ideal process sequence is represented by the reference sequence x_0(k). Higher grey relational grade therefore indicates that the related parameters combination is nearer to the ideal.

5.3 OPTIMIZATION BY USING MULTI OBJECTIVE GREY -BASED TAGUCHI METHOD FOR L9 TAGUCHI ORTHOGONAL ARRAY DESIGN OF EXPERIMENT

In order to normalize the experimental data using the equation 5.4, the responses (ultimate tensile strength and breaking tensile strength) of the L_9 Taguchi orthogonal array design of experiment should be high. Experimental data are gathered in accordance with the chapter 3 and chapter 4-discussed L_9 Taguchi orthogonal array design matrix. Table 5.1 displays the experimental data after normalisation.

Table: 5.1 Normalisation of experimental data using an experiment with a L_9 Taguchi Orthogonal Array

Exp No.	Ultimate Tensile Strength (MPa) Larger is better	Elongation percentage (%) Larger is better
1	0.0000	1.0000
2	0.7681	0.5346
3	1.0000	0.5161
4	0.4169	0.4147
5	0.4775	0.1959
6	0.3167	0.2765
7	0.8981	0.3756
8	0.1586	0.9217
9	0.3540	0.0000

Table 5.2 Calculation of grey relational coefficients ($\xi_i(k)$)

Exp No.	Ultimate Tensile Strength (MPa)	Elongation percentage (%)
1	0.3333	1.0000
2	0.6832	0.5179
3	1.0000	0.5082
4	0.4616	0.4607
5	0.4890	0.3834
6	0.4225	0.4087
7	0.8307	0.4447
8	0.3727	0.8645
9	0.4363	0.3333

Grey relation grades for all performance characteristics have been calculated by using equation 5.7

Table 5.3 Calculation of overall-grey relation grade

Exp No.	Grey Relation Grade	Rank
1	0.6667	2
2	0.6005	5
3	**0.7541**	1

4	0.4612	6
5	0.4362	7
6	0.4156	8
7	0.6377	3
8	0.6186	4
9	0.3848	9

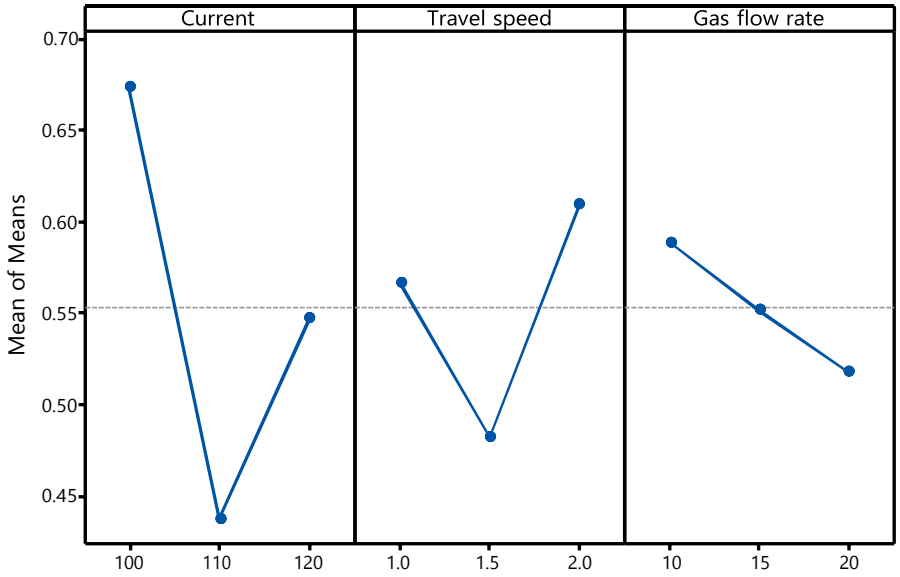

Figure 5.1: Main effect plot for overall grey relation grade

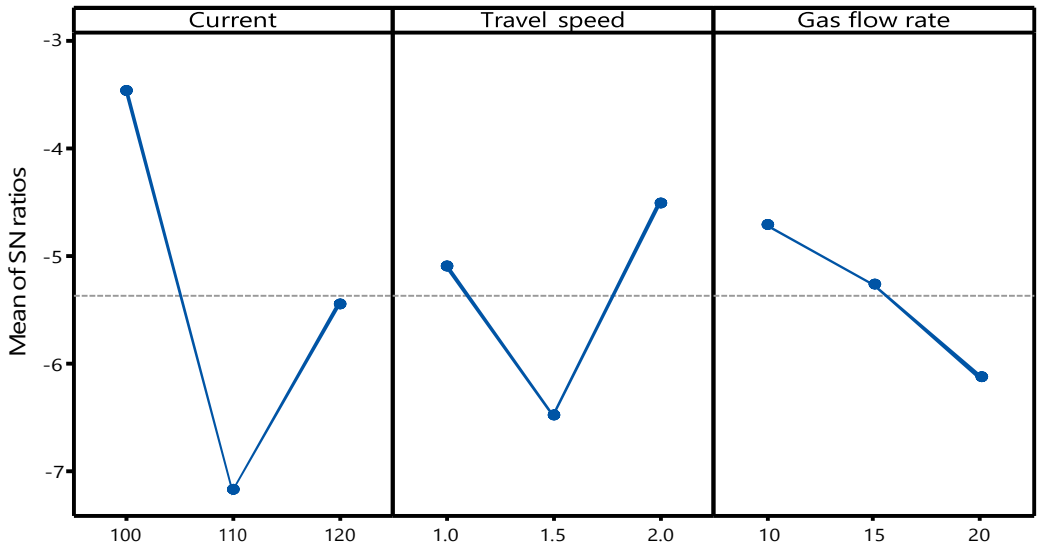

Signal-to-noise: Larger is better

Figure 5.2: Main effect plot for overall grey relation grade

With the help of mean effect plot for S/N ratio and main effect plot for means (Figure 5.1 and Figure 5.2), optimum parametric combination has been determined.

Table 5.4 Mean value table for overall grey relation grade

Level	Current	Travel speed	Gas flow rate
1	**0.6738**	0.5670	**0.5885**
2	0.4377	0.4822	0.5518
3	0.5470	**0.6093**	0.5182
Delta	0.2361	0.1272	0.0704
Rank	1	2	3

Mean value of overall of overall grey relational grade indicates the order of factors (ranking) representing the extent of significance on the overall grey relational grade.

Optimization:

Table 5.5 Optimization solutions

Solution	Current	Gas flow rate	Travel speed	GRG	Composite Desirability
1	100	10	2	0.765989	1

Table 5.6 ANOVA table for Overall Grey relation grade

Source	DF	Adj SS	Adj MS	F-Value	P-Value	Percentage Contribution
Current	2	0.083766	0.041883	4.19	0.193	61.44
Gas flow rate	2	0.007432	0.003716	0.37	0.729	5.45
Travel speed	2	0.025157	0.012579	1.26	0.443	18.45
Error	2	0.019987	0.009993			
Total	8	0.136342				

Analysis of variance of overall grey relation grade shown that % of contribution in case of welding current is more with respect to travel speed and gas flow rate. Since P value is not less than 0.05 so none of the factors are not significant.

CHAPTER 6

CONCLUSIONS AND FUTURE SCOPE OF WORK

6.1 CONCLUSIONS

Welding of Austenitic stainless steel by TIG: Based on the results of investigation and analyses, the followings conclusions are made.

- Visual inspection and an X-ray radiography test show that a small number of samples had flaws such porosity, lack of fusion, and undercut. Under particular parametric conditions, joints with nearly no defects are also seen.
- Except for a few samples, the results of the tensile test are determined to be satisfactory. The mechanical properties have been somewhat impacted by changes in the input parameters. The range of ultimate tensile strength (UTS) is 398 to 586 MPa.
- According to measurements of hardness at various weldment zones, weld metal is harder than base metal and HAZ metal. The HAZ hardness is discovered to be somewhat lower than basic metal. However, it is not believed that the range in hardness in various zones is overly great.
- The microstructure of base metal has a substantial amount of austenitic twin and is entirely austenitic. In comparison to the microstructure of base metal, no appreciable differences are seen in the microstructure of HAZ. But in HAZ, grain growth is visible. In HAZ, austenitic twins are also seen, and the weld metal has equiaxed grain. There is also columnar dendritic development in some samples. The findings of the tensile test are often consistent with micro structural features.
- Current 110A, gas flow rate 20 liters/min, and travel speed 3 mm are the parameters that are judged to be ideal. This is the result of multi-objective optimization utilizing the Grey-based Taguchi approach to simultaneously maximize UTS and PE.
- Through ANOVA, the significance of each factor has been determined. Welding current is the most important element.

6.2 FUTURE SCOPE OF WORK

- The welding parameters of current, gas flow rate, and arc gap have all been altered in the current investigation. It is also possible to include additional factors like voltage, welding speed, and filler rod diameter. This outlines the range of upcoming work.

- The TIG welding of several other austenitic stainless-steel kinds (i.e., types other than 304 types) may be the subject of experiments.

- The data from the current study may be used to create a trustworthy Artificial Neural Network model for response prediction given a set of input parameters, if more trial runs are required.

- The thickness of austenitic stainless steel employed in this investigation is 3 mm. The study could be expanded to include other material thicknesses (smaller and larger).

- The impact of process parameters with modifications in edge preparation may also be investigated in connection to TIG welding of stainless steel.

- In the current work, the study of weld microstructures has only been somewhat explored. It goes without saying that a crucial area to be further researched in the future for TIG welding of austenitic stainless steel is the impact of process parameters on the microstructures of the weldment.

- Future research opportunities include the determination of HAZ width, the hardness of the various weldment zones, weld-metal chemistry, and many others.

- Data analysis and process parameters optimization can be done using a variety of established and cutting-edge approaches, and the value of each technique can be assessed.

Reference

[1] Ramkumar, K. D.; Chandrasekhar, A.; Singh, A. K.; Ahuja, S.; Agarwal, A.; Arivazhagan,N.; Rabel, A. M. Comparative Studies on the Weldability, Microstructure and Tensile Properties of Autogeneous TIG Welded AISI 430 Ferritic Stainless Steel with and without Flux. *J. Manuf. Process.* 2015, *20*, 54–69. https://doi.org/10.1016/j.jmapro.2015.09.008.

[2] Vora, J. J.; Badheka, V. J. Experimental Investigation on Microstructure and Mechanical Properties of Activated TIG Welded Reduced Activation Ferritic/Martensitic Steel Joints. J. Manuf. Process. 2017, 25, 85–93. https://doi.org/10.1016/j.jmapro.2016.11.007.

[3] Rajput, S. K.; Kumar, A.; Tripathi, S. S.; Sachan, E. Investigation of Microstructural Behavior and Mechanical Properties of Dissimilar Weld Joints of Austenitic-Ferritic Stainless Steel. *Mater. Today* 2020, *25*, 778–784. https://doi.org/10.1016/j.matpr.2019.09.018.

[4] Vidyarthy, R. S.; Dwivedi, D. K.; Vasudevan, M. Influence of M-TIG and A-TIG Welding Process on Microstructure and Mechanical Behavior of 409 Ferritic Stainless Steel. *J. Mater. Eng. Perform.* 2017, *26* (3), 1391–1403. https://doi.org/10.1007/s11665-017-2538-5.

[5] Raveendra, A.; Ravi Kumar, B. V. Experimental Study on Pulsed and Non- Pulsed Current TIG Welding of Stainless Steel Sheet(SS304). *International Journal of Innovative Research in Science, Engineering and Technology* 2013.

[6] Sivaprasad, K.; Raman, S. G. S. Influence of Magnetic Arc Oscillation and Current Pulsing on Fatigue Behavior of Alloy 718 TIG Weldments. *Mater. Sci. Eng. A Struct. Mater.* 2007, *448* (1–2), 120–127. https://doi.org/10.1016/j.msea.2006.10.048.

[7] Roy, A.; Ghosh, N.; Mondal, S. Effect of Heat Input on Mechanical and Metallurgical Properties of AISI 304L Stainless Steel by Using TIG Welding. *Weld. Int.* 2023, 1–10. https://doi.org/10.1080/09507116.2023.2185169.

[8] Ghosh, N.; Pal, P. K.; Nandi, G. Investigation on Dissimilar Welding of AISI 409 Ferritic Stainless Steel to AISI 316L Austenitic Stainless Steel by Using Grey Based Taguchi

Method. Adv. Mater. Process. Technol. 2018, 4 (3), 385–401. https://doi.org/10.1080/2374068x.2018.1451182.

[9] Anttila, S.; Karjalainen, P.; Lantto, S. Mechanical Properties of Ferritic Stainless-Steel Welds in Using Type 409 and 430 Filler Metals. Weld. World 2013. https://doi.org/10.1007/s40194-013-0033-7.

[10] Lothongkum, G.; Viyanit, E.; Bhandhubanyong, P. Study on the Effects of Pulsed TIG Welding Parameter on Delta-Ferrite Content, Shape Factor and Bead Quality in Orbital Welding of AISI 316L Stainless Steel Plate. J. Mater. Process. Technol. 2001, 110 (2), 233–238. https://doi.org/10.1016/s0924-0136(00)00875-x.

[11] Vidyarthy, R. S.; Dwivedi, D. K. Analysis of the Corrosion Behaviour of an A-TIGWelded SS 409 Weld Fusion Zone. J. Mater. Eng. Perform. 2017, 26 (11), 5375–5384. https://doi.org/10.1007/s11665-017-3022-y.

[12] Kumar, H.; Ahmad, G. N.; Singh, N. K. Activated Flux TIG Welding of Inconel 718 Super Alloy in Presence of Tri-Component Flux. Mater. Manuf. Process. 2019, 34 (2), 216–223. https://doi.org/10.1080/10426914.2018.1532581.

[13] Vidyarthy, R. S.; Dwivedi, D. K. Weldability Evaluation of 409 FSS with A-TIG Welding Process. Mater. Today 2019, 18, 3052–3060. https://doi.org/10.1016/j.matpr.2019.07.177.

[14] Ambade, S.; Kataria, R.; Tembhurkar, C.; Meshram, D. Experimental and Finite Element Analysis of Temperature Distribution in 409 M Ferritic Stainless Steel by TIG, MIG and SMAW Welding Processes. Adv. Mater. Process. Technol. 2022, 1–16. https://doi.org/10.1080/2374068x.2022.2100127.

[15] Lakshminarayanan, A. K.; Shanmugam, K.; Balasubramanian, V. Effect of Welding Processes on Tensile and Impact Properties, Hardness and Microstructure of AISI 409M Ferritic Stainless Joints Fabricated by Duplex Stainless Steel Filler Metal. J. Iron Steel Res. Int. 2009, 16 (5), 66–72. https://doi.org/10.1016/s1006-706x(10)60013-1.

[16] Narang, H. K.; Singh, U. P.; Mahapatra, M. M.; Jha, P. K. Prediction of the Weld Pool Geometry of TIG Arc Welding by Using Fuzzy Logic Controller. Int. J. Eng. Sci. Technol. B, Lagos 2012, 3 (9), 77–85. https://doi.org/10.4314/ijest.v3i9.6.

[17] Gupta, S. K.; Raja, A. R.; Vashista, M.; Yusufzai, M. Z. K. Effect of Heat Input on Microstructure and Mechanical Properties in Gas Metal Arc Welding of Ferritic Stainless Steel. Mater. Res. Express 2018, 6 (3), 036516. https://doi.org/10.1088/2053- 1591/aaf492.

[18] Köse, C.; Topal, C. Effect of Post Weld Heat Treatment and Heat Input on the Microstructure and Mechanical Properties of Plasma Arc Welded AISI 410S Ferritic Stainless Steel. Mater. Res. Express 2019, 6 (6), 066517. https://doi.org/10.1088/2053- 1591/ab09b6.

[19] Amuda, M. O. H.; Mridha, S. Effect of Energy Input on Microstructure and Hardness of TIG Welded AISI 430-Ferritic Stainless Steel. Adv. Mat. Res. 2011, 264–265, 390–396. https://doi.org/10.4028/www.scientific.net/amr.264-265.390.

[20] Prakash Pasupulla, A.; Abebe Agisho, H.; Seetharaman, S.; Vijayakumar, S. Characterization and Analysis of TIG Welded Stainless Steel 304 Alloy Plates Using Radiography and Destructive Testing Techniques. Mater. Today 2022, 51, 935–938. https://doi.org/10.1016/j.matpr.2021.06.305.

[21] Yan, J.; Gao, M.; Zeng, X. Study on Microstructure and Mechanical Properties of 304 Stainless Steel Joints by TIG, Laser and Laser-TIG Hybrid Welding. Opt. Lasers Eng. 2010, 48 (4), 512–517. https://doi.org/10.1016/j.optlaseng.2009.08.009.

[22] Durgutlu, A. Experimental Investigation of the Effect of Hydrogen in Argon as a Shielding Gas on TIG Welding of Austenitic Stainless Steel. Mater. Eng. 2004, 25 (1), 19–23. https://doi.org/10.1016/j.matdes.2003.07.004.

[23] Aslam, M.; Sahoo, C. K. Numerical and Experimental Investigation for the Cladding of AISI 304 Stainless Steel on Mild Steel Substrate Using Gas Metal Arc Welding. CIRP J. Manuf. Sci. Technol. 2022, 37, 378–387. https://doi.org/10.1016/j.cirpj.2022.02.017.

[24] Kumar, S.; Shahi, A. S. Effect of Heat Input on the Microstructure and Mechanical Properties of Gas Tungsten Arc Welded AISI 304 Stainless Steel Joints. Mater. Eng. 2011, 32 (6), 3617–3623. https://doi.org/10.1016/j.matdes.2011.02.017.

[25] Shanmugam, K.; Lakshminarayanan, A. K.; Balasubramanian, V. Effect of Weld Metal Properties on Fatigue Crack Growth Behaviour of Gas Tungsten Arc Welded AISI 409M Grade Ferritic Stainless-Steel Joints. Int. J. Pressure Vessels Piping 2009, 86 (8), 517–524. https://doi.org/10.1016/j.ijpvp.2009.02.002.

[26] Mahajan, A.; Singh, H.; Kumar, S.; Kumar, S. Mechanical Properties Assessment of TIG Welded SS 304 Joints. Mater. Today 2022, 56, 3073–3077. https://doi.org/10.1016/j.matpr.2021.12.133.

[27] Wang, Q.; Sun, D. L.; Na, Y.; Zhou, Y.; Han, X. L.; Wang, J. Effects of TIG Welding Parameters on Morphology and Mechanical Properties of Welded Joint of Ni-Base Superalloy. Procedia Eng. 2011, 10, 37–41. https://doi.org/10.1016/j.proeng.2011.04.009.

[28] IRJET Journal. Irjet-Review on the Parametric Optimizaton of Tig Welding. 2017

[29] Zhou, J.; Shen, J.; Hu, S.; Zhao, G.; Wang, Q. Microstructure and Mechanical Properties of AISI 430 Ferritic Stainless Steel Joints Fabricated by Cold Metal Transfer Welding. *Mater. Res. Express* 2019, *6* (11), 116536. https://doi.org/10.1088/2053-1591/ab4770.

[30] Vidyarthy, R. S.; Dwivedi, D. K. Analysis of the Corrosion Behavior of an A-TIG Welded SS 409 Weld Fusion Zone. J. Mater. Eng. Perform. 2017, 26 (11), 5375–5384. https://doi.org/10.1007/s11665-017-3022-y.

[31] Mousazadeh, M. A.; Derakhshandeh-Haghighi, R. Autogenous Tungsten Inert Gas Welding of 430 Ferritic Stainless Steel: The Effect of Inter-Pass Temperature on Microstructure Evolution and Mechanical Properties. J. Mater. Eng. Perform. 2020, 29 (12), 7807–7820. https://doi.org/10.1007/s11665-020-05281-z.

[32] Lakshminarayanan, A. K.; Balasubramanian, V.; Madhusudhan Reddy, G. Microstructure and Mechanical Properties of Electron Beam-Welded AISI 409M-Grade Ferritic Stainless Steel. Int. J. Adv. Manuf. Technol. 2011, 55 (1–4), 153–162. https://doi.org/10.1007/s00170-010-3044-1.

[33] Akita, M.; Uematsu, Y.; Kakiuchi, T.; Nakajima, M.; Agata, Y.; Takino, K. Joint Microstructures, Mechanical Properties and Fatigue Behaviour of Ferritic Stainless-Steel SUS 430 Welds with Different Filler Metals. Weld. Int. 2018, 32 (6), 427–435. https://doi.org/10.1080/09507116.2017.1346860.

[34] Mohandas, T.; Madhusudhan Reddy, G.; Naveed, M. A Comparative Evaluation of Gas Tungsten and Shielded Metal Arc Welds of a “Ferritic” Stainless Steel. J. Mater. Process. Technol. 1999, 94 (2–3), 133–140. https://doi.org/10.1016/s0924-0136(99)00092-8.

[35] Lakshminarayanan, A. K.; Balasubramanian, V. An Assessment of Microstructure, Hardness, Tensile and Impact Strength of Friction Stir Welded Ferritic Stainless-Steel Joints. Mater. Eng. 2010, 31 (10), 4592–4600. https://doi.org/10.1016/j.matdes.2010.05.049.

[36] Lakshminarayanan, A. K.; Balasubramanian, V. Process Parameters Optimisation for Friction Stir Welding of AISI 409M Grade Ferritic Stainless Steel. Exp. Tech. 2013, 37 (5), 59–73. https://doi.org/10.1111/j.1747-1567.2011.00802.x.

[37] Dinaharan, I.; Muthu Krishnan, T.; Palanivel, R. An Assessment of Microstructure and Tensile Behavior of Magnetically Impelled Arc Butt Welded AISI 409 Ferritic Stainless-Steel Tubes. J. Mater. Eng. Perform. 2022, 31 (10), 7808–7819. https://doi.org/10.1007/s11665-022-06806-4.

[38] Ambriz, R. R.; Delgado, J. A.; Cuenca-Álvarez, R.; Alatorre, N.; Curiel, F. F. Heat Input Effect on the Microstructural Transformation and Mechanical Properties in GTAW Welds of a 409L Ferritic Stainless Steel. Rev. Metal. 2016, 52 (2), e068. https://doi.org/10.3989/revmetalm.068.

[39] Ambriz, R. R.; Delgado, J. A.; Cuenca-Álvarez, R.; Alatorre, N.; Curiel, F. F. Heat Input Effect on the Microstructural Transformation and Mechanical Properties in GTAW Welds of a 409L Ferritic Stainless Steel. Rev. Metal. 2016, 52 (2), e068. https://doi.org/10.3989/revmetalm.068.

[40] Zaman, S.; Khattak, M. A.; Tamin, M. Effects of Welding on the Microstructural Properties of AISI 43 Ferritic Stainless Steel. 2018.

[41] Ambriz, R. R.; Delgado, J. A.; Cuenca-Álvarez, R.; Alatorre, N.; Curiel, F. F. Heat Input Effect on the Microstructural Transformation and Mechanical Properties in GTAW Welds of a 409L Ferritic Stainless Steel. Rev. Metal. 2016, 52 (2), e068. https://doi.org/10.3989/revmetalm.068.

[42] Ghosh, N.; Kumar, P.; Nandi, G. Parametric Optimization of Gas Metal Arc Welding Process by Using Grey Based Taguchi Method on Aisi 409 Ferritic Stainless Steel. Technol. Eng. 2016, 13 (1), 6–11. https://doi.org/10.2478/teen-2016-0003.

[43] Ghosh, N.; Kumar Pal, P.; Nandi, G.; Rudrapati, R. Parametric Optimization of Gas Metal Arc Welding Process by PCA Based Taguchi Method on Austenitic Stainless Steel AISI 316L. Mater. Today 2018, 5 (1), 1620–1625. https://doi.org/10.1016/j.matpr.2017.11.255.

[44] Ghosh, N.; Pal, P. K.; Nandi, G. Parametric Optimization of MIG Welding on 316L Austenitic Stainless Steel by Grey-Based Taguchi Method. Procedia Technol. 2016, 25, 1038–1048. https://doi.org/10.1016/j.protcy.2016.08.204.

[45] Ibrahim, I. A.; Mohamat, S. A.; Amir, A.; Ghalib, A. The Effect of Gas Metal Arc Welding (GMAW) Processes on Different Welding Parameters. Procedia Eng. 2012, 41, 1502–1506. https://doi.org/10.1016/j.proeng.2012.07.342.

[46] Karadeniz, E.; Ozsarac, U.; Yildiz, C. The Effect of Process Parameters on Penetration in Gas Metal Arc Welding Processes. Mater. Eng. 2007, 28 (2), 649–656. https://doi.org/10.1016/j.matdes.2005.07.014.

[47] Kim, I. S.; Son, J. S.; Park, C. E.; Kim, I. J.; Kim, H. H. An Investigation into an Intelligent System for Predicting Bead Geometry in GMA Welding Process. J. Mater. Process. Technol. 2005, 159 (1), 113–118. https://doi.org/10.1016/j.jmatprotec.2004.04.415.

[48] Sharma, A.; Verma, A.; Vashisth, D.; Khanna, P. Prediction of Bead Geometry Parameters in MIG Welded Aluminium Alloy 8011 Plates. Mater. Today 2022, 62, 2787–2793. https://doi.org/10.1016/j.matpr.2022.02.063.

[49] Narang, R.; Maheshwari, V.; Khanna, P. Prediction of Bead Geometry Parameters in MIG Welded Stainless Steel 409L Plates by Mathematical Modelling. Mater. Today 2021, 44, 900– 908. https://doi.org/10.1016/j.matpr.2020.10.795.

[50] Kumar, H.; Singh, N. K. Performance of Activated TIG Welding in 304 Austenitic Stainless- Steel Welds. Mater. Today 2017, 4 (9), 9914–9918. https://doi.org/10.1016/j.matpr.2017.06.293.

[51] Ghosh, A,: Mallick, A. k. Manufacturing Science; Ellis Horwood Ltd, publisher: Harlow, England, 1986.

[52] Rao. Manufacturing Technology: Foundry, Forming and Welding, 2nd Ed,: McGraw-Hill Education: London, England, 1999.

[53] https://www.idconline.com/technical_references/pdfs/mechanical_engineering/The_principle_Of_Tungsten_Inert_Gas_TIG_Welding_Process.pdf